BARRY, JEREMY ALAN, M.S. Separation of Alzheimer's Disease Biomarkers Using a Nanoparticle Pseudostationary Phase In Capillary Electrophoresis. (2010) Directed by Dr. Brent Dawson. 91 pp.

Alzheimer's Disease (AD) is the most common form of senile dementia and affects millions of people worldwide. Patients with AD suffer from progressive memory loss that is caused by the loss of neurons and synapses in the portions of the brain responsible for memory and cognitive ability.[1] AD is characterized by the formation of senile plaques made mostly of the Amyloid Beta peptide and neurofibrillary tangles consisting of the Tau protein. The onset of AD seems to be correlated with changes in the concentrations of the Amyloid Beta peptides and the Tau protein.[2] The relative concentrations of $A\beta_{42}$ to $A\beta_{40}$ and the total amount of Tau can be used as biomarkers for the early detection of AD.[3] A fast, multianalyte analysis of these biomarkers could provide useful information in the diagnosis of the disease as well as a means of tracking disease progression. Capillary electrophoresis is a fast separations technique that allows for the separation of analyte based on the size to charge ratio. This technique coupled with laser-induced fluorescence is capable of picomolar limits of detection. This study focuses on a novel functionalized gold nanoparticle enhanced capillary electrophoresis technique for the separation and quantitation these Alzheimer's Disease biomarkers.

SEPARATION OF ALZHEIMER'S DISEASE BIOMARKERS USING A

NANOPARTICLE PSEUDOSTATIONARY PHASE

IN CAPILLARY ELECTROPHORESIS

by

Jeremy Alan Barry

A Thesis Submitted to
the Faculty of The Graduate School at
The University of North Carolina at Greensboro
in Partial Fulfillment
of the Requirements for the Degree
Master of Science

Greensboro
2010

Approved by

_____
Committee Chair

To my parents John and Joanne

APPROVAL PAGE

This thesis has been approved by the following committee of the Faculty of The

Graduate School at The University of North Carolina at Greensboro.

Committee Chair   _____

Committee Members   _____

_____

_____
Date of Acceptance by Committee

_____
Date of Final Oral Examination

ACKNOWLEDGEMENTS

TABLE OF CONTENTS

LIST OF TABLES

LIST OF FIGURES

ABBREVIATIONS

Aβ-- amyloid beta
ACN -- acetonitrile
AD --- Alzheimer's Disease
ADDLs --- amyloid derived diffusible ligands
APP -- amyloid precursor protein
CE-- capillary electrophoresis
CEC--- capillary electrochromatography
CMC-- critical micelle concentration
CSF -- cerebrospinal fluid
CZE--- capillary zone electrophoresis
DMSO--- dimethyl sulfoxide
DMF-- dimethyl formamide
DPD--- dipyridyl disulfide
ELISA -- enzyme linked immunosorbant assay
ESI -- electrospray ionization
FTIR -- fourier transform infrared radiation
HPLC --- high performance liquid chromatography
KCN -- potassium cyanide
LIF -- laser-induced fluorescence
LOD--- limit of detection
LSPR-- localized surface plasmon resonance
MALDI-- matrix assisted laser desorption/ionization
MDS -- mercaptodecanesulfonate
MEKC--- micellar electrokinetic chromatography
MS -- mass spectrometer
NFT--- neurofibrillary tangle
NMR--- nuclear magnetic resonance
pTau--- phosphorylated tau protein
SAM -- self assembled monolayer
SDS --- sodium dodecyl sulfate
SPR --- surface plasmon resonance
TIC-- total ion chromatogram
THF--- tetrahydrofuran
TOF--- time of flight
tTau --- total amount of tau protein
UV-Vis --- ultra violet-visible
3D-SAM-- three dimensional self assembled monolayer

CHAPTER I

INTRODUCTION

Statement of Problem

There are currently an estimated 24 million people worldwide that have been

diagnosed with Alzheimer's Disease. Aside from being the most prevalent

neurodegenerative disease, it is also the third most expensive disease costing the United

States over $100 billion dollars annually.[4] There is currently no definitive diagnosis

other than an autopsy. Prevalence of Alzheimer's Disease is correlated with changes in

cerebrospinal fluid concentrations of the amyloid beta peptides and tau protein. A high

throughput method that is used to determine the concentration of these biomarkers in

cerebrospinal fluid would assist in assigning a more definitive diagnosis and to track

disease progression.

Chapter Overview

For quantitation of each of the amyloid beta peptides to be possible, they must

first be separated. This project involved the production of a pseudostationary phase in a

capillary electrophoretic analysis to separate these peptides. The pseudostationary phase

consisted of 10 nm gold nanoparticles functionalized with an asymmetric disulfide, 10-

(dodecyldisulfanyl) decane-1-sulfonic acid. Because this disulfide is not commercially

available, its synthesis and characterization was required.

This project began with the synthesis of a sulfonic acid terminated alkyl thiol, mercaptodecanesulfonate (MDS). Following the purification of MDS as well as its characterization using NMR spectroscopy, MDS was reacted with dodecanethiol to form an asymmetric disulfide. This coupling was accomplished through the use of a disulfide exchange reaction. The characterization of the asymmetric disulfide was carried out using NMR spectroscopy and FTIR spectroscopy.

The synthesized disulfide was then used to derivatize 10 nm gold nanoparticles. The optimal disulfide concentration and derivatization time was determined by allowing a range of disulfide concentrations to react with the nanoparticles over time. Characterization of the self-assembled monolayer of the disulfide on the gold surface was achieved through tracking the shift in the plasmon band using visible absorbance and FTIR spectroscopy.

The detection method for the analysis of the selected biomarkers was laser-induced fluorescence which required the biomarkers to be derivatized with a fluorescent dye. The amyloid beta peptides were derivatized with an amine reactive fluorescent dye. The conditions were optimized to get preferential attachment of the dye to the N-terminus of each peptide with minimal attachment to the two lysine side chains on both peptides. The number of dye molecules on each peptide was determined by MALDI mass spectrometry. The tau protein was derivatized using a thiol reactive dye because it is a large protein that has too many possible reactive sites for an amine reactive dye. The tau protein contains only one cysteine as opposed to 37 possible amine reactive sites making a thiol reactive dye more selective for a single attachment.

The sulfonic acid functionalized nanoparticles that have been made in this research as well as the carboxylic acid functionalized nanoparticles that were synthesized prior to this research project were used to effect the separation of the amyloid beta peptides, and the tau protein, as well as a mixture of all three biomarkers. The conditions of the separation including the type of buffer, pH, and voltage setting were optimized for the detection of the biomarkers.

CHAPTER II

REVIEW OF THE LITERATURE

Capillary Zone Electrophoresis

Capillary electrophoresis (CE) involves the movement of ions in a capillary, through the application of an electric field.[5] A typical CE system consists of a capillary, an injector, a high voltage power supply, electrodes, as well as some form of detection. Some of the various detection schemes will be discussed in greater detail later. The capillary is where the separation takes place. The capillary is made of fused silica that is roughly 330 µm thick with an inner diameter of 25-75 µm. Generally, the capillaries are 50 cm in length from inlet to the detection window and are coated with a polyimide coating to make them more durable. At the detector, the polyimide coating is "burned" off to make a detection window for on column detection. At either end, the capillary sits in a vial of buffer solution. These vials also contain platinum electrodes which are connected to a high voltage power source. The circuit between the electrodes is completed in the capillary using a conductive electrolyte solution, normally a 50 mM buffer solution.

The power supply, which is normally set between 5-30 kV, produces the electric field which provides the means for the differential migration of analyte ions in solution. The ions in solution will have different electrophoretic mobilities depending on their size to charge ratios. Those ions that are of similar size will then be separated according the magnitude of their charge. When the electric field is applied, the analyte ions will

migrate towards the cathode or anode depending on their charge. Anions in solution will travel in the direction of the anode, which is normally at the inlet. Cations will migrate to the cathode, which is at the outlet. The velocity at which each ion travels is inversely proportional to its hydrodynamic radius and proportional to the strength of the applied field and the charge on the ion. This velocity is considered to be the ions electrophoretic velocity.

Another factor that affects the movement of the analyte is the electroosmotic flow. Electroosmotic flow can be described as the flow of solvent in an electric field. In CE, electroosmosis is highly dependent on pH, concentration, and composition of the background electrolyte.[6] The interior of the capillary has exposed silanol groups (SiOH) which can be deprotonated above pH 3. This gives the inner wall of the capillary an overall negative charge. Cations in the buffer solution will be attracted to the capillary walls and will form a double layer to neutralize the charge on the wall. When the electric field is applied, the cation rich double layer will flow towards the cathode. The double layer provides a more plug like flow profile because the flow is generated from the wall. This plug like flow profile is beneficial when compared to the parabolic flow profile that arises from pressure driven systems, like high performance liquid chromatography (HPLC), that leads to band broadening. The apparent mobility of an ion in capillary electrophoresis is the sum of its electrophoretic and electroosmotic mobility. The electroosmotic mobility must be greater than the electrophoretic mobility of the anions in order for them to be detected. In a configuration where the anode was at the inlet and the cathode was at the outlet, cations would elute before neutral compounds which would

elute before anions. Cations would elute first because they possess electrophoretic and electroosmotic mobility toward the detector. The anions are negatively charged so they will be attracted to the positively charged anode which is at the inlet. Since the anions are attracted to the anode at the inlet, they will spend more time in the capillary and will elute last. The neutral analyte will be carried through the capillary at the velocity of the electroosmotic flow. With this configuration the anions will have an apparent mobility that is slower than the electroosmotic flow, cations will have an apparent mobility that is faster than the electroosmotic flow, and neutral analytes will have an apparent mobility that is equal to the electroosmotic flow.

Detection in Capillary Electrophoresis

There is an array of detection schemes that can be used with capillary electrophoresis. Detection systems are analyte dependent, so each method has its advantages and its drawbacks. The most used detection methods include absorbance, fluorescence, mass spectrometry will be discussed below. However, there are other detection methods such as potentiometric, conductivity, amperometric, and refractive index.

Direct Absorbance

The most common detector for CE separations is the absorbance detector. It works well with compounds that have native absorbance including many organic compounds, since most of them will absorb around 195-210 nm. The buffers used must then have little absorbance in this region. One of the major drawbacks of UV absorbance detection is that it is limited by Beer's Law. The magnitude of the pathlength is a major component of the sensitivity of absorbance measurements. However, in CE the

pathlength of the capillary is so small, 25-75 µm, that there must be an appreciable

amount of chromophoric analyte present for detection. The concentration limit of

detection for direct absorbance in capillary electrophoresis is 10^{-5}-10^{-6} M.[7] Methods have

been developed to improve detection by increasing the pathlength at the detection

window. Z-cells allow for the absorbance measurement to be taken along the length of

the capillary in the detection window. Even though this increases the sensitivity, it also

increases the length of the sample band to the point where peaks must be separated by the

length of the flow cell or they will overlap. Another way to increase the pathlength is to

use a bubble cell, in which the diameter of the capillary at the detector is increased. A

different method uses a multireflection cell where two windows are made on opposite

sides of the capillary about 1.5cm apart. Between them is a silver coating that reflects the

laser light from the entrance window through the capillary to the exit window where the

absorbance measurement is made.[8] Even with the extended pathlength, the concentration

limit of detection for absorbance is still around 10^{-6} M.[3] Ultimately, absorbance

measurements are restricted by Beer's law and the difficulties associated with measuring

small changes in signal against a large background.

Indirect Absorbance

Another configuration for the absorbance detector is to take indirect absorbance

measurements. Indirect absorbance is a way to detect analytes that have very little

absorptivity. The buffer contains an absorbing species that produce a high background

signal. The non-absorbing analyte displace the absorbing species to produce a signal in

the form of an inverse peak. The advantage of this technique is that it does not require

derivatization of non-UV-absorbing species.

Direct On-column Laser-induced Fluorescence

The most sensitive method of detection in capillary electrophoresis is laser-induced fluorescence (LIF). The concentration LOD for on-column LIF is 10^{-13} M for chemically derivatized samples and 10^{-11} M for natively fluorescent analyte.[9] One of the more sensitive arrangements entails the angle between the excitation laser and fluorescence collection to be zero degrees. In one common configuration an argon ion laser is focused into a fiber optic cable which illuminates the capillary. This illumination is realized by focusing the laser onto a dichroic mirror which reflects the light at the excitation wavelength onto the capillary. The emission wavelength from the analyte will pass back through the dichroic mirror and emission filters to a photomultiplier tube. Having an angle of zero degrees between the excitation and collection reduces the scattering by the walls of the capillary. This arrangement leads to a lower background and enhancement of the fluorescence signal.[10]

For on-column detection, non-fluorescent analyte molecules are chemically derivatized with a fluorophore prior to CE analysis. There is a wide selection of fluorescent probes that react with various functional groups including biological thiols and primary amines. Perhaps one of the biggest drawbacks to chemical derivatization is that it can lead to multiple labeling of an analyte that has more than one reactive site. Multiple labeling of analytes will cause a difference in their electrophoretic mobility since the label adds mass and will often times neutralize charge. While multiple reaction sites will increase the signal, the distribution of analytes with different degrees of derivatization will lead to multiple peaks for a single analyte.[11] There have been techniques developed to circumvent this problem. Pinto and coworkers added a

submicellar concentration of SDS to the buffer which effectively homogenized the multiply labeled protein analyte to a single peak.[12] The probe involved reacted with primary amines allowing it to attach to the N-terminus or ε-amine side chains leading to a mixture of derivatized products. The sulfate group of the submicellar SDS interacts with the underivatized primary amines making them effectively neutral and adds approximately the same mass as the fluorescent probe. The SDS corrects for the different numbers of attached probes and gives analytes of the same type roughly the same electrophoretic mobility so they will migrate under the same peak. The other technique for avoiding the problem of multiple derivatizations is to conduct a post-capillary derivatization which falls under the category of post column detection.

Direct Post-column Laser-induced Fluorescence

The detection limit for post-column fluorescence is as low as 10^{-16} M, which is considered single molecule detection.[3] Post-column fluorescence techniques will normally involve a sheath flow cuvette which eliminates the Raleigh and Raman scattering from the capillary. Passing through the cuvette is a buffer which matches the refractive index of the sample to decrease scattering that would be caused by a refractive index mismatch and the sheath flow helps hydrodynamically focus the fluorescence signal.[13] The signal is focused to a pinhole through which the fluorescent emission is collected, which further reduces scattering. Post column detection also allows for post-capillary derivatization. In this technique, the analyte is derivatized in a reaction cell or capillary just prior to detection. This method requires less sample prep before analysis, but requires a fluorogenic reagent that has fast reaction kinetics. Fluorogenic probes are

those that are fluorescent only after reaction with the analyte to avoid a high background

signal.[14]

Indirect Laser-induced Fluorescence
Indirect LIF is very similar to the method for indirect absorbance that was

previously described. Yeung and Kuhr were the first to employ this technique using a

background buffer that fluoresces to detect species that do not exhibit native

fluorescence.[15] The non-fluorescent analyte displaces the fluorescent buffer to produce a

decrease in the fluorescent signal, or an inverse peak. The detection limits for this

method are very poor (10^{-6} M) when compared with other fluorescence detection

techniques because the background is fairly noisy. This is due to instability in the laser

intensity. The benefit of this setup is that it does not require chemical derivatization.

Mass Spectrometry
There are two major categories of mass spectrometric (MS) detectors for CE.

There are online and offline detectors. There are a variety of different interfaces to

connect the two instruments. Electrospray ionization is the most popular online means of

coupling the CE separation with MS. Perhaps one of the more sensitive systems,

designed by Mazereeuw *et al.*, has a tapered outlet on the separation capillary that is

positioned in front of the MS inlet so that the applied field for the separation also acts to

generate the electrospray. There is an electrical contact between the tip of the capillary,

through the air, to the MS which is grounded.[16] This setup uses a single high voltage

power supply to effect the separation and to produce the electrospray or microspray in

this case. The LOD for this method is in the nanomolar range. Other ESI interfaces use a

sheath flow at the end of the capillary. Often times the optimized conditions for the

separation don't match the optimized conditions for the MS portion of the experiment. The sheath flow interface resolves this problem, allowing the buffer conditions in the sheath flow to be optimized for ionization just prior to entering the MS. The matrix-assisted laser desorption/ionization mass spectrometer (MALDI-MS) is used as an offline MS detection method for CE. The eluent is continuously deposited on a membrane surface that is coated with MALDI matrix.[17] This arrangement is effective, but there is some loss of the separation efficiency. Even though MS detectors are not as sensitive as some of the other detection schemes like fluorescence, they provide qualitative as well as quantitative information about the analyte, often giving positive identification of the analyte.

Micellar Electrokinetic Chromatography

One major drawback of traditional capillary electrophoresis or CZE is that it does not allow the separation of neutral species. The neutral analyte molecules will travel in the same band and will have the same migration as the electroosmotic flow since they do not have an electrophoretic mobility. One way to circumvent this problem is to conduct micellar electrokinetic chromatography (MEKC).[18] This mode of CE involves the addition of a surfactant above its critical micelle concentration (cmc) to form micelles. Above the cmc, the surfactant will aggregate to form micelles that have their polar head groups toward the aqueous phase, and their hydrophobic tails toward each other. Sodium dodecyl sulfate (SDS) is commonly used in MEKC and will be used as an example here. Once the sample is loaded, the electric field is applied. The portion of the micelle that is exposed to the buffer has negative charge from each of the deprotonated sulfate groups. The negative charge of the sulfate group causes the micelle to have an electrophoretic

mobility that is towards the anode/inlet. Analyte that interacts with the micelle will travel

at the velocity of the micelle during the time spent in the micelle. This interaction

effectively slows the migration time of that analyte. The more interaction that takes

place, the longer the migration time will be. Even though the micelles are not bonded to

the interior of the capillary, they function the same as a stationary phase in

chromatography and are given the name pseudostationary phase. In MEKC, the analyte

is separated according to two mechanisms. The first mechanism is the difference in the

electrophoretic mobility. The second mechanism of separation is the analyte's

partitioning in the hydrophobic core of the micelle. By this mechanism, MEKC can

separate neutral compounds as well as compounds that have similar electrophoretic

mobilities. Since there is a fairly high concentration of surfactant that is present in the

eluent, compatibility with MS can be problematic. The presence of surfactant micelles

can greatly reduce the sensitivity of the MS. A solution to this problem has been

developed where a plug of micelles is injected near the inlet of the capillary. The analyte

must then migrate through a plug of micelles then on to the electrophoresis buffer before

entering the mass spectrometer.[19]

Capillary Electrochromatography

Capillary electrochromatography (CEC) is a mode of CE separation that combines

the selectivity of HPLC with the resolution and efficiency of CE.[20] In CEC the

capillaries are monolithic or packed with small diameter particles or porous beads. The

packings are similar to those used in HPLC but smaller diameter particles (<1µm) can be

used. One of the bigger problems facing CEC is that it is difficult to pack such small

particles into a small column in a reproducible manner. Another drawback to using such

small particles is that it decreases the sample loading capacity of the column. In CEC, it is the electroosmotic flow that drives the analyte through the column, not pressure like in HPLC, meaning that the flow profile is flat and plug-like instead of parabolic, which leads to more efficient separations. The separation of charged species is dependent on the electroosmotic flow, the electrophoretic mobility, as well as the partitioning of the analyte into the stationary phase. For a neutral analyte, the migration will be dependent on the electroosmotic mobility and the partitioning of the analyte in the stationary phase. Like in HPLC, frits are required on either end of the capillary to keep the particles in the column. These frits tend to cause band broadening and lead to bubble formation. The bubbles are caused by a slight difference in the electroosmotic flow at the interface between the packed and unpacked portions of the capillary. Bubble formation is particularly detrimental in CEC because it will stop the electrical current. This adverse effect can be overcome by applying pressure at both ends of the capillary or by using monolithic columns.[21]

Monolithic columns are networks of crosslinked polymer that form a single rod. These columns do not require the use of frits to retain the stationary phase in the capillary. In CEC the walls of the capillary are bare so the exposed silanol groups will lead to the adsorption of basic analytes. The silanols could be end-capped, however that would lead to a reduction in the electroosmotic flow. CEC, in a way, combines the best of both worlds in having the benefits of having the high efficiency of CE and high selectivity of HPLC.

Nanoparticles

The use of nanoparticles in separation science is becoming an increasingly popular trend. This tendency is most likely due to the fact that nanoparticles have a high surface area to volume ratio which is favorable in chromatography due to minimization of the resistance to mass transfer. The nanoparticles can be functionalized with various functional groups depending on the surface chemistry of the particle. The most common nanoparticles are made from polymers, silica, and gold. Gold nanoparticles possess a great deal of promise since they are highly stable and have excellent optical sensitivity which are advantageous properties for chemical derivatization.[22] The affinity of gold for organosulfur compounds, more specifically alkylthiols and dialkyldisulfides, makes functionalization of gold surfaces particularly straightforward. Other metals in the same periodic group, such as silver and copper, also possess the same chemisorption properties but are more easily oxidized. The chemisorption of thiols or disulfides onto gold surfaces has been shown to produce highly ordered monolayers.[23] The generation of these self-assembled monolayers (SAMs) through the adsorption of organosulfur compounds onto two dimensional surfaces is a well studied area.[24] The properties of the monolayers can be varied by changing the functional group on the ω-position of the alkyl thiol. Mixtures of thiols that have different terminal groups can be used to produce a mixed monolayer that has various functionalities on the surface of the gold. The problem with this method is that the distribution of each type of thiol onto the surface isn't necessarily solely dependent on its concentration in the mixture. Smaller chain alkyl thiols on the gold surface are more likely to be replaced by longer chain alkyl thiols with more methylene groups.[25] The chemisorption of asymmetric disulfides allows for even better control over

the homogeneity of the surface coverage because the gold surface induces the cleavage of the sulfur-sulfur bond to form thiolate bonds with the gold.[26] It was demonstrated that both halves of an asymmetric disulfide were present in equal proportions on the gold surface after chemisorption.[27] The principles involved in the production of SAMs are similar to those applied in the chemisorption of organosulfur compounds onto three dimensional particles (3D-SAMs). The replacement of thiols on the surface of nanoparticles is dependent on the relative amount of the thiol and whether or not it increases the stability of the particle. In other words, the thiol that promotes increased stability of the nanoparticle will display higher expression on the gold surface. In the formation of 3D-SAMs, monolayers from a mixture of thiols, the degree of adsorption of each thiol is dominated by which promotes the stability of the particle, which implies thermodynamic control. On the contrary, the composition of the monolayer that is formed from mixed disulfides is more inherently controlled by the kinetics of the reaction at the gold surface.[28] This implies that disulfide chemisorption allows for better control over the surface properties of the gold.

Characterization of the monolayers on the gold surface can be achieved through a variety of methods. The degree of disulfide adsorption onto the gold nanoparticles can be monitored by tracking the local surface plasmon band. A plasmon is merely a quantum of plasma oscillation that is comparable to what a photon is to light. At the metal surface there is a density of free electrons because of the fixed positive ions in the metal. Under irradiation with light the oscillating electromagnetic field from a photon of light causes the electrons to undergo oscillation with respect to the positive metal surface.[29] For a

nanoparticle, the frequency of light at which this process is resonant is called the

localized surface plasmon resonance (LSPR).[30] This oscillation decays by either

radiating its energy through scattering (Mie scattering) or by nonradiative conversion of

the absorbed light into heat.[31] For the noble metals, this absorption occurs in the visible

region.[32] Surface plasmons are very sensitive to changes that occur at the interface

between the metal and surrounding solvent (water).[33] The adsorption of the disulfide

causes a red shift in the maxima of the surface plasmon band due to the increase in the

relative size of the particle and because of the change in the refractive index at the

gold/water interface as the thiolates are formed. Characterization of the thiolates on the

particle surface can be realized through FTIR or NMR spectroscopy. The ^{13}C and ^{1}H

NMR of functionalized gold nanoparticles shows characteristically broader peaks

compared to that of the free disulfide or thiol. This phenomenon is believed to be due to

the slower rotational velocity of the particle.[34] FTIR spectra of alkylthiolates on gold

particles also have characteristic peaks. The spectra look similar to the spectra of the free

thiol or disulfide with a few noticeable differences. As the monolayer begins to order

itself through lateral van der Waals interactions with adjacent methylenes, defects can

form. An increase in the number of defects causes a shift in the C-H stretching vibrations

to higher energies.[35] Compared to the FTIR spectra of the free thiol/disulfide, the

chemisorbed thiolates will have lower energy C-H stretches. The characterization of the

functionalized gold nanoparticles using these methods will be necessary prior to use as a

pseudo stationary phase in CE experiments.

Alzheimer's Disease

In order to emphasize the possible impact of this study, it is important to be familiar with the underlying progression of Alzheimer's Disease. Alzheimer's Disease (AD) is a neurodegenerative disease that affects an estimated 24 million people worldwide.[36] The prevalence of the disease increases with age and with the increased aging population, AD is becoming a more prominent problem. The only definitive diagnosis for AD involves an autopsy for the presence of the pathological hallmarks. The trademarks of Alzheimer's Disease are the formation of neurofibrillary tangles of hyperphosphorylated Tau protein and amyloid plaques of the Amyloid Beta peptide in the brain. The pathology of AD is still somewhat ambiguous, but there are two major theories as to the cause of the disease. The two pathways are the Amyloid Beta hypothesis and the Tau hypothesis.

Amyloid Beta Hypothesis

The Amyloid Beta peptide (Aβ) is a cleavage product of a transmembrane protein called the Amyloid Precursor Protein (APP). There are three secretases that cleave APP: the α-secretase, β-secretase, and γ-secretase (Figure 1). They each cleave the protein at different sites. There are two processing pathways for APP involving these three secretases: an amyloidogenic pathway and a non-amyloidogenic pathway. The amyloidogenic pathway leads to the formation of the Aβ peptide and is the more prominent pathway in patients with AD. The β-secretase cleaves the APP on the extracellular domain at one end of the Aβ peptide sequence. This is followed by the subsequent cleavage of APP in the membrane spanning region by the γ-secretase. The γ-secretase cleaves at the other end of the Aβ sequence, releasing it into the extracellular

space outside the neuron. The non-amyloidogenic pathway, which is thought to be the dominant pathway in healthy individuals, starts with APP cleavage by the α-secretase. The α-secretase cleaves APP in the middle of the sequence of what would be the Aβ peptide . Then the γ-secretase cleaves APP in the membrane spanning region. It is important to note that this pathway does not lead to production of the Aβ peptide. The γ-secretase has the ability to cleave APP in a couple of locations to produce varying lengths

Figure 1. Proteolytic Cleavage of APP

Cleavage Sites of Transmembrane Portion of APP

β-secretase   α-secretase   γ-secretase

...KMDAEFRHDSGYEVHHQKLVFFAEDVGSNKGAIIGLMVGGVVIATBIBITL...

DAEFRHDSGYEVHHQKLVFFAEDVGSNKGAIIGLMVGGVV   Aβ1-40

DAEFRHDSGYEVHHQKLVFFAEDVGSNKGAIIGLMVGGVVIA   Aβ1-42

of Aβ (37-42 amino acids) in the amyloidogenic pathway. The $Aβ_{1-40}$ is the more common, less toxic form of Aβ. When the γ-secretase cleaves APP after 42 amino acids, it liberates the more hydrophobic and more harmful $Aβ_{1-42}$. This form of the peptide is more prone to aggregation. When it is released, it starts to adhere to other $Aβ_{1-42}$ and forms soluble assemblies called amyloid derived diffusible ligands (ADDLs). The ADDLs collect more of the $Aβ_{1-42}$ making them increasingly insoluble. They are then believed to attach to a receptor site on the dendrite which is responsible for receiving messages from other neurons. Being unable to communicate, the neuron loses function

and eventually dies. Ultimately they grow to form insoluble amyloid plaques which are

one of the hallmarks of AD. It is now believed that the soluble oligomers of $A\beta_{1-42}$ are

more toxic than the insoluble plaques or deposits.[37] As the peptides aggregate, their

relative concentrations in solution will start to decrease. The amyloid beta cascade is the

more supported hypothesis. Mutations in APP have been shown to lead to increased

formation of $A\beta_{1-42}$. This fact implies that there is genetic control over formation of $A\beta_{1-42}$ which may lead to plaque formation. There have also been studies that suggest $A\beta$ has

a connection to Tau phosphorylation. One study demonstrated that Amyloid deposits

may be modulated by lithium which is also a Tau protein kinase inhibitor.[38] Another

study showed that $A\beta_{1-42}$ can bind to the Tau protein and promote its phosphorylation.[39]

This observation provides support to the theory that the amyloid beta cascade precedes

the Tau pathology.

Tau Hypothesis

The Tau protein is the other biomarker that is involved in AD. The normal

function of Tau is to stabilize microtubules in nerve cells. The phosphorylation of the

Tau protein and other microtubule associated proteins causes them to detach from the

microtubule and leads to its destabilization. Phosphorylation of these proteins is used in

the cell as a mechanism for the regulation of microtubule stabilization. In AD an

increased hyperphosphorylation of the Tau proteins leads to a substantial detachment

from the microtubule and results in the destabilization of the microtubules in nerve cells.

Tau phosphorylation also makes it less susceptible to proteolysis.[40] As

hyperphosphorylated tau proteins increase in number they begin to aggregate and form

neurofibrillary tangles (NFTs). The accumulation of these tangles in the neuron results in

neuronal death.[41] Tau has also been deemed responsible for other forms of dementia. This is why some believe that it is Tau that is responsible for the neuronal degeneration in AD.[42] It is almost certain that both the amyloid beta aggregation and hyperphosphorylated Tau are responsible for neuronal death, but the question of which comes first still remains.

Biomarkers

Changes in biochemical processes in the brain can be reflected in the cerebrospinal fluid (CSF) since it is in direct contact with the extracellular space of the central nervous system. The concentrations of the AD biomarkers ($A\beta_{1-42}$, $A\beta_{1-40}$, pTau, tTau) in the CSF can then be used as a means tracking disease progression or to assist with providing a more accurate diagnosis of AD. It has been shown that there is a direct correlation between the concentrations of these biomarkers and the onset of AD. In patients that have AD there is a characteristic increase in the total amount of Tau protein (tTau) in CSF as well as an increase in the CSF concentration of Tau that is phosphorylated at threonine 181 (pTau). There is also a decrease in the relative amount of $A\beta_{1-42}$ that is found in CSF.[43] These findings are consistent with the proposed mechanisms since hyperphosphorylation of Tau leads to its dissociation from microtubules increasing its concentration in the CSF, and increased production of $A\beta_{1-42}$ leads to its aggregation in the brain leading to a decrease in $A\beta_{1-42}$ concentration. It has been shown that the ratio of $A\beta_{1-42}/A\beta_{1-40}$ is better associated with the disease than just the $A\beta_{1-42}$ concentration alone.[44] Currently the tests for these biomarkers are done using an Enzyme-linked immunosorbant assay (ELISA). Some of the drawbacks associated with using this technique are that each test is very time consuming because of its single

analyte nature so multiple tests would be required to analyze each of the biomarkers. Also, cross-reactivity can lead to false positives and false negatives. The use of antibodies in these ELISA tests causes the tests to be fairly expensive and entail strict control over conditions such as pH for valuable results. There is also a great deal of disagreement in values that are obtained from different antibody based tests.[45] A high throughput analysis for the determination of the relative amounts of these biomarkers can greatly assist in a more accurate diagnosis of AD as well as provide a means for tracking progression of the disease. There are currently treatments for AD that are in clinical trials, so fast and accurate clinical assays for these biomarkers could also offer information about the efficacy of these treatments.

CHAPTER III

SYNTHESIS AND CHARACTERIZATION OF ASYMMETRIC DISULFIDE

Introduction

The use of thiols and disulfides in the production of highly ordered self assembled monolayers on gold surfaces is a well defined area of research.[46] The use of disulfides in particular allows for the production of a monolayer that can have various functionalities. In synthesizing functionalized nanoparticles that are to be used in the separation of the AD biomarkers, a selective interaction between the biomarkers and nanoparticles would be beneficial. The disulfide that is chemisorbed onto the surface of the nanoparticle should then consist of at least one alkyl chain that acts as a point of hydrophobic interaction for the biomarkers. This, in essence, gives the particle reversed phase character. It is advantageous if the monolayer of the functionalized nanoparticles had charge associated with it to give the particle an electrophoretic mobility and a point of ionic exchange. The use of a sulfonic acid as the ω-functionality provides this charged character. The advantage of using a sulfonic acid functionality is that it is deprotonated at almost every pH giving a higher abundance of negative character to the nanoparticles over a wide pH range. The disulfide shown in Figure 2 was chosen to be synthesized and used in the functionalization of gold nanoparticles because it has the properties that would be useful in this type of separation. The synthesis of the disulfide required the synthesis of an alkyl sulfonic acid terminated with a thiol. This thiol was then reacted with an alkyl thiol via a disulfide exchange reagent.

**Figure 2. 10-(dodecyldisulfanyl) decane-1-sulfonic acid**
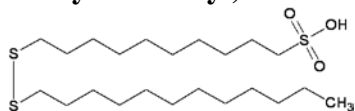
Materials and Methods

The chemicals used in the syntheses were obtained from the following companies: Acros Organics (thiourea, 1-dodecanethiol); Alfa Aesar (1,10-dibromodecane, 2,2'-dipyridyldisulfide); Cambridge Isotope Laboratories (deuterated methanol, deuterated dimethylsulfoxide, deuterium oxide); Fisher Scientific (acetone, ethyl ether, petroleum ether, potassium bromide, sodium hydroxide, sodium sulfite); Pharmco-AAPER (ethanol (90%), ethanol (200 proof)).

Because the chosen disulfide is not available commercially, it had to be synthesized. The synthesis of the asymmetric disulfide began with the production of the functional arm that contains the sulfonic acid. This functional arm is a sulfonic acid terminated alkyl thiol known as mercaptodecanesulfonate (MDS) shown in Figure 3.

Figure 3. Mercaptodecanesulfonate (MDS)
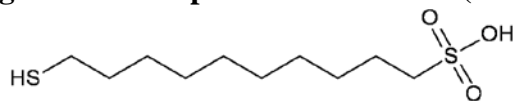
The synthesis of MDS was slightly modified from that reported by Fiurasek and Reven.[47] The scheme for the synthesis of MDS is shown in Figure 4 below. A 5 molar excess of dibromodecane (42.4490 g, 0.141 mol) was added to a mixture of 60 mL of 95% ethanol and 20 mL of nanopure water in a 500 mL triple-neck round bottom flask. This mixture was heated to reflux (~80˚C) while being stirred. Sodium sulfite (3.5500 g,

0.0277 mol) was dissolved in 40 mL of nanopure water and was added to a 125 mL

pressure equalizing addition funnel. The sodium sulfite solution was added dropwise to

the refluxing dibromodecane mixture over a period of 3 hours in an effort to only react

one end of the dibromodecane. After refluxing for an additional 4 hrs the excess

dibromodecane was separated from the reaction mixture. The aqueous portion was

washed with three 25 mL portions of petroleum ether to remove the unreacted

dibromodecane. The aqueous portion was then concentrated by rotary evaporation to

remove the ethanol. The resulting solution was cold crystallized and the resultant crystals

were collected by vacuum filtration. The compound was verified by proton NMR to be

sodium 10-bromodecanesulfonate (Figure 6). The mass of the sodium 10-

bromodecanesulfonate was 7.0735 g giving a yield of 96%. The subsequent reaction

involved dissolving the 10-bromodecanesulfonate (7.0735 g, 0.0219 mol) in a mixture of

75 mL of 200 proof ethanol and 25 mL of nanopure water in a 250 mL round bottom

flask. An equimolar amount of thiourea (1.6314 g, 0.0219 mol) was added to the mixture

and the reaction was brought up to reflux (~78˚C) and stirred for 6 hours. The reaction

mixture was then concentrated to 25 mL by rotary evaporation and cold crystallized

giving 5.8692 g of product which relates to a 90% yield. The resulting solid was

confirmed by proton NMR to be 10-S-thiouronium decanesulfonate (Figure 7). 10-S-

thiouronium decanesulfonate (5.8692 g, 0.0198 mol) was then dissolved in 60 mL of 10

mM sodium hydroxide in a 250mL round bottom flask and submitted to a base hydrolysis

to cleave the C-S bond releasing the alkylthiol and urea. The reaction was refluxed (~

93˚C) and stirred for three hours under an argon stream. After three hours the reaction

mixture was taken off the heat and allowed to cool without stirring overnight under argon

stream. The thiol was protonated by acidification with dilute sulfuric acid (0.7 mL of

concentrated sulfuric acid to 5 mL of water) which was added dropwise to the stirring

mixture until a pH of 7 was reached. The solution was then cooled on ice and the

resultant crystals were obtained by vacuum filtration. The product had a mass of 4.8828

g (97%) and was verified by proton NMR (Figure 8), ^{13}C NMR (Figure 11), FTIR (Figure

12), and HPLC-ESI-MS to be Mercaptodecanesulfonic acid (MDS)(Figure 9, Figure 10).

Figure 4. MDS Synthetic Scheme
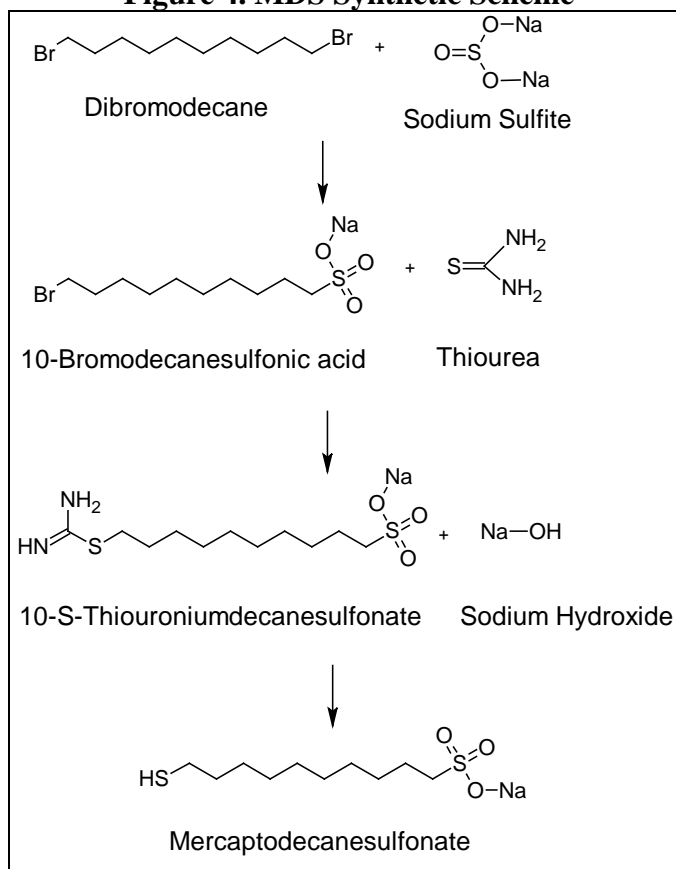
The formation of asymmetric disulfides has been demonstrated using thiol-disulfide exchange reagents. These compounds form a disulfide bond with one thiol and act as a good leaving group for reaction with a subsequent thiol to produce the desired asymmetric disulfide. The most popular thiol-disulfide exchange reagents are the pyridyl disulfides.[48] One such compound, 2, 2'-dipyridyldisulfide, has been shown to act as a thiol-disulfide exchange reagent in the production of asymmetric disulfides.[49] The thiol made in the prior synthesis, MDS, was reacted with a four molar excess of 2, 2'-dipyridyldisulfide (Figure 5). The MDS (74 mg, 0.292mmol) was dissolved in a mixture of 20 mL of nanopure water and 5 mL of acetone and added to a 125 mL pressure equalized addition funnel. The 2,2'-dipyridyldisulfide (240 mg, 1.09 mmol) was dissolved in 15 mL of acetone and added to a 100 mL round bottom flask. The MDS solution was added dropwise to the stirring 2,2'-dipyridyldisulfide mixture at room temperature over a period of three hours to reduce the chance of the subsequent reaction with the product to form the symmetric disulfide. When the MDS thiol reacts with the 2, 2'-dipyridyldisulfide (DPD) it produced the mixed disulfide MDS-pyridyldisulfide and releases pyridine-2-thione. This reaction product, pyridine-2-thione, is spectrophotometrically measureable at 343 nm. This allowed for the reaction progress to be tracked by UV absorbance (Figure 13). Once the absorbance reached a maximum at 343 nm, the reaction was completed. The reaction took an additional 4 hours after all of the MDS was added to reach completion. The excess DPD and pyridine-2-thione was washed from the reaction mixture using ethyl ether. The reaction mixture was then concentrated by rotary evaporation to 20 mL and cold crystallized to give 84 mg of

product, equivalent to a 75% yield. The product was verified by proton NMR to be

MDS-pyridyldisulfide. The MDS-pyridyldisulfide (84 mg, 0.219 mol) was then

dissolved in 20 mL of nanopure water and was reacted with an equimolar amount of

dodecanethiol (44 mg, 0.219 mol) dissolved in 20 mL of acetone to produce the

asymmetric disulfide. This reaction also produces the pyridine-2-thione byproduct that

allows for tracking of the reaction to completion. Upon completion, the pyridine-2-

thione was washed from the reaction mixture using three 10 mL portions of ethyl ether

and both the aqueous and organic layers were dried for NMR analysis. The aqueous

layer consisted mainly of the 10-(dodecyldisulfanyl) decane-1-sulfonic acid (Figure 14).

The organic layer consisted mostly of pyridine-2-thione and unreacted dodecanethiol.

The 10-(dodecyldisulfanyl) decane-1-sulfonic acid was then analyzed by FTIR (Figure

15).

Figure 5. 10-(dodecyldisulfanyl) decane-1-sulfonic acid Synthetic Scheme
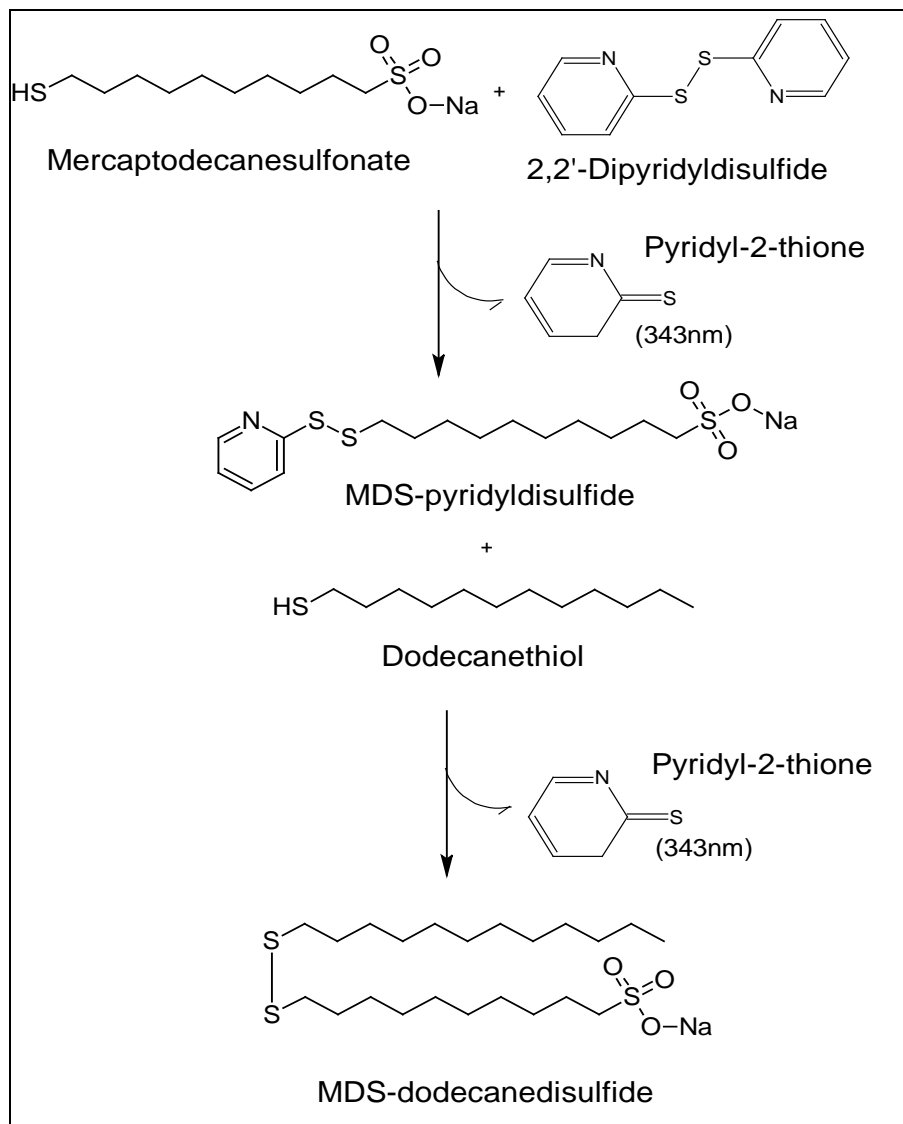

Results

    ^{1}H and ^{13}C NMR were obtained by dissolving 10 mg of the compound of interest

in 0.75 mL of the appropriate deuterated solvent (deuterium oxide, deuterated methanol,

or deuterated dimethyl sulfoxide). All NMR were obtained using a JEOL 500 MHz

spectrometer. Fourier Transform Infrared analysis was conducted using a Nicolet Nexus

470 FTIR. Sample preparation for FTIR involved adding 5 mg of sample to 200 mg of

dried potassium bromide and which was then pressed into a KBr pellet. UV Absorbance

measurements were made using a Cary 100 Bio UV-Visible Spectrophotometer by

Varian.

Figure 6 displays the proton NMR of the first synthetic product in the synthesis of

MDS. The first peak around 1.3 ppm corresponds to the methylene peak, the next group

of peaks at 1.8 ppm is two overlapped quintuplets corresponding to the protons beta to

the sulfonic acid and bromine. The triplet at 2.7 ppm is the protons alpha to the sulfonic

acid and the triplet at 3.4 ppm is the protons alpha to the bromine. The peak in between

the triplets at 3.29 ppm is a solvent peak.

Figure 6. Proton NMR of 10-Bromodecanesulfonate
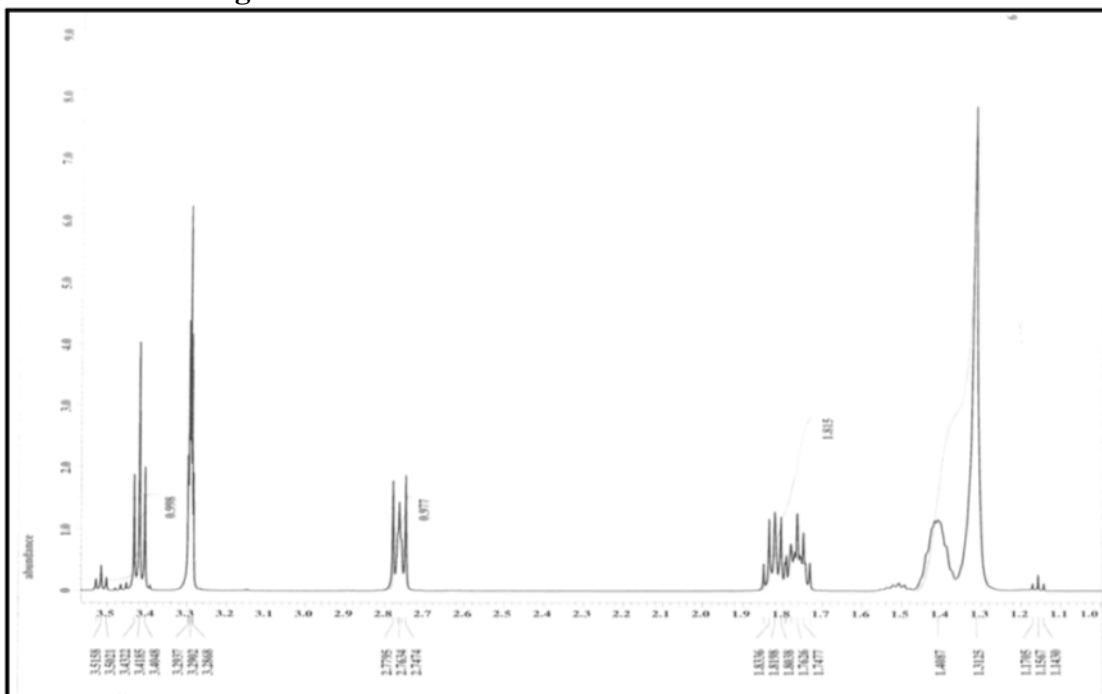
1H NMR (Methanol D-3) δ 1.3-1.4 (m, 12H, -CH$_2$CH$_2$(C**H**$_2$)$_6$CH$_2$CH$_2$-), 1.7-1.8 (m, 4H,
SO$_3$CH$_2$C**H**$_2$(CH$_2$)$_6$C**H**$_2$CH$_2$Br), 2.76 (t, 2H, -CH$_2$C**H**$_2$SO$_3$), 3.40 (t, 2H, -CH$_2$C**H**$_2$Br)

Figure 7 shows the proton NMR of the second product in the MDS synthesis. The

peaks at around 1.3 ppm are the methylene peaks, there are two overlapping quintuplets

at 1.5-1.6 ppm for the protons beta to the thiouronium and sulfonic acid. The triplet at

2.4 ppm is the protons alpha to the sulfonic acid. The triplet at 3.1 ppm is due to the

protons alpha to the thiouronium and the doublet at 9.0 ppm is due to the protons on the

nitrogens.

Figure 7. Proton NMR of Thiouroniumdecanesulfonate
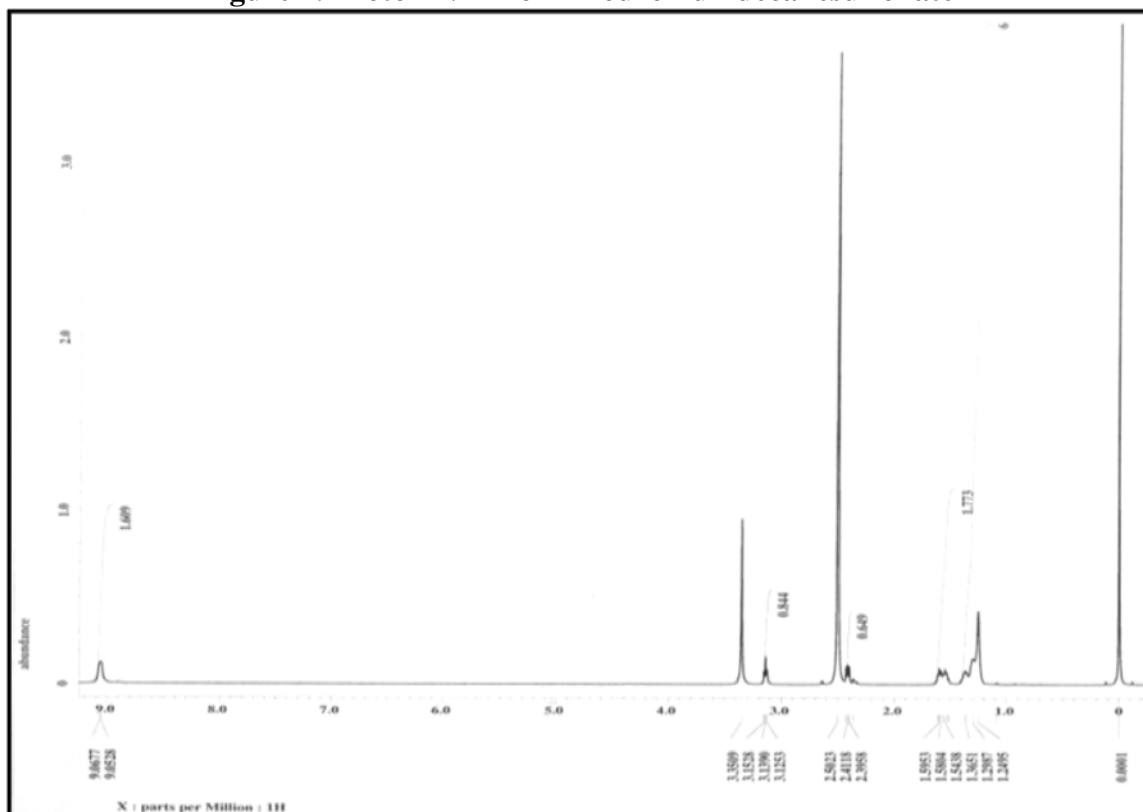
1H NMR (Methanol D-3) δ 1.2-1.4 (m, 12H, -CH$_2$CH$_2$(CH$_2$)$_6$CH$_2$CH$_2$-), 1.5-1.6 (m, 4H,
SO$_3$CH$_2$CH$_2$(CH$_2$)$_6$CH$_2$CH$_2$SC(NH$_2$)$_2$), 2.41 (t, 2H, -CH$_2$CH$_2$SO$_3$), 3.13 (t, 2H, -CH$_2$CH$_2$
SC(NH$_2$)$_2$), 9.06 (d, 4H, - CH$_2$CH$_2$ SC(NH$_2$)$_2$)

Figure 8 shows the proton NMR of the thiol product mercaptodecanesulfonate. The methylene peaks are at around 1.3 ppm. The quintuplet at 1.52-1.57 ppm is due to the protons beta to the thiol. The next quintuplet at 1.65-1.71 ppm is due to the protons beta to the sulfonic acid. The triplet at 2.49 ppm is due to the protons alpha to the thiol. The triplet at 2.85 ppm corresponds to the protons alpha to the sulfonic acid.

Figure 8. Proton NMR of Mercaptodecanesulfonate
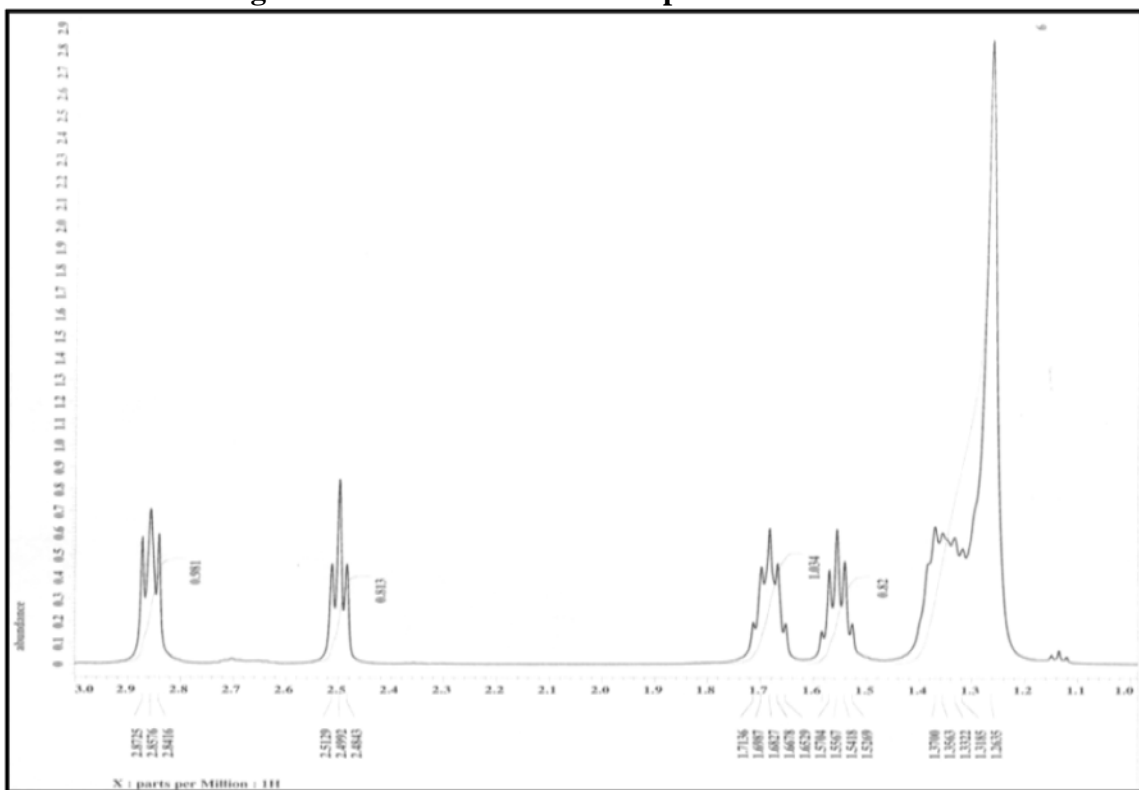
1H NMR (D$_2$O) δ 1.2-1.4 (m, 12H, -CH$_2$CH$_2$(C**H$_2$**)$_6$CH$_2$CH$_2$-), 1.5-1.6 (m, 2H, -C**H$_2$**CH$_2$SH), 1.65-1.75 (m, 2H, -C**H$_2$**CH$_2$SO$_3$), 2.49 (t, 2H, -CH$_2$C**H$_2$**SH), 2.85 (t, 2H, -CH$_2$C**H$_2$**SO$_3$)

Figure 9 shows the total ion chromatogram of the product MDS. This compound was run on an HPLC connected to a mass spectrometer with an electrospray ionization source. This figure shows the compound eluting after 37.28 minutes with a mass of 252.19. This particular run was completed in negative mode.

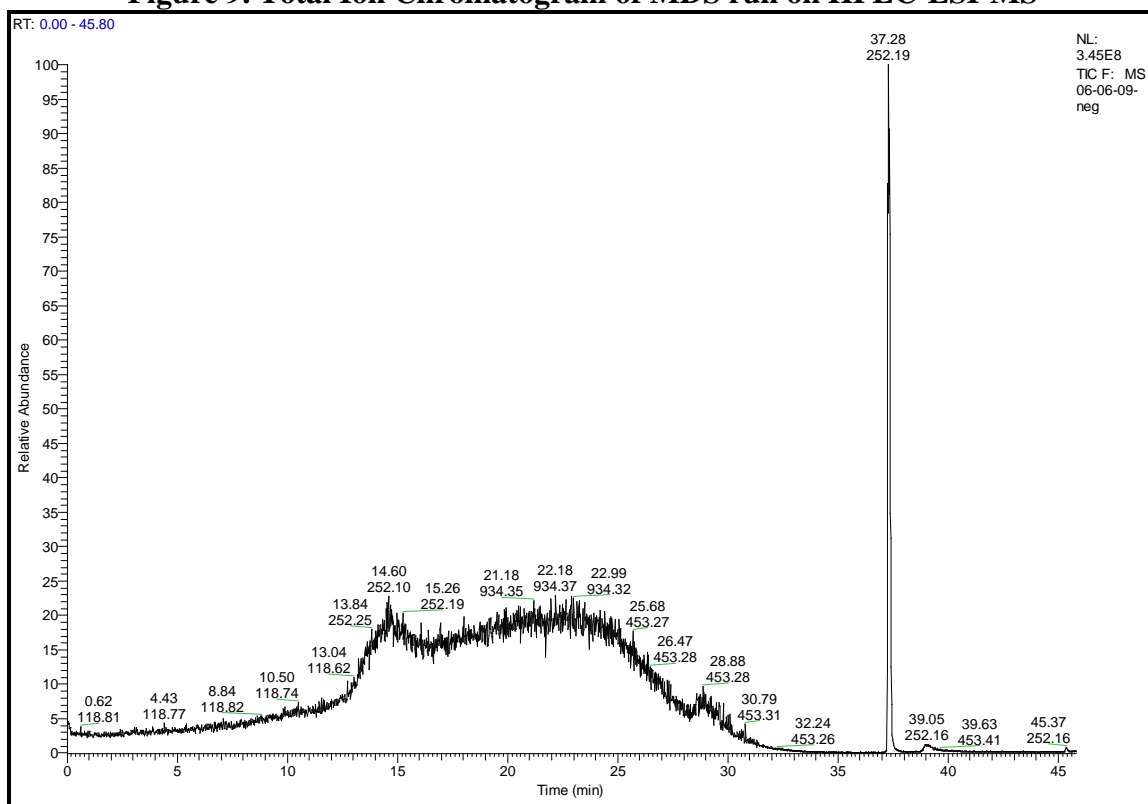**Figure 9. Total Ion Chromatogram of MDS run on HPLC-ESI-MS**

Figure 10 shows the mass spectrum of the peak at 37.28 minutes in the total ion chromatogram shown above. The major peak in this spectrum is shown at 252.19 m/z suggesting the mass of the compound to be 252.19 g/mol. This spectrum was taken in negative mode.

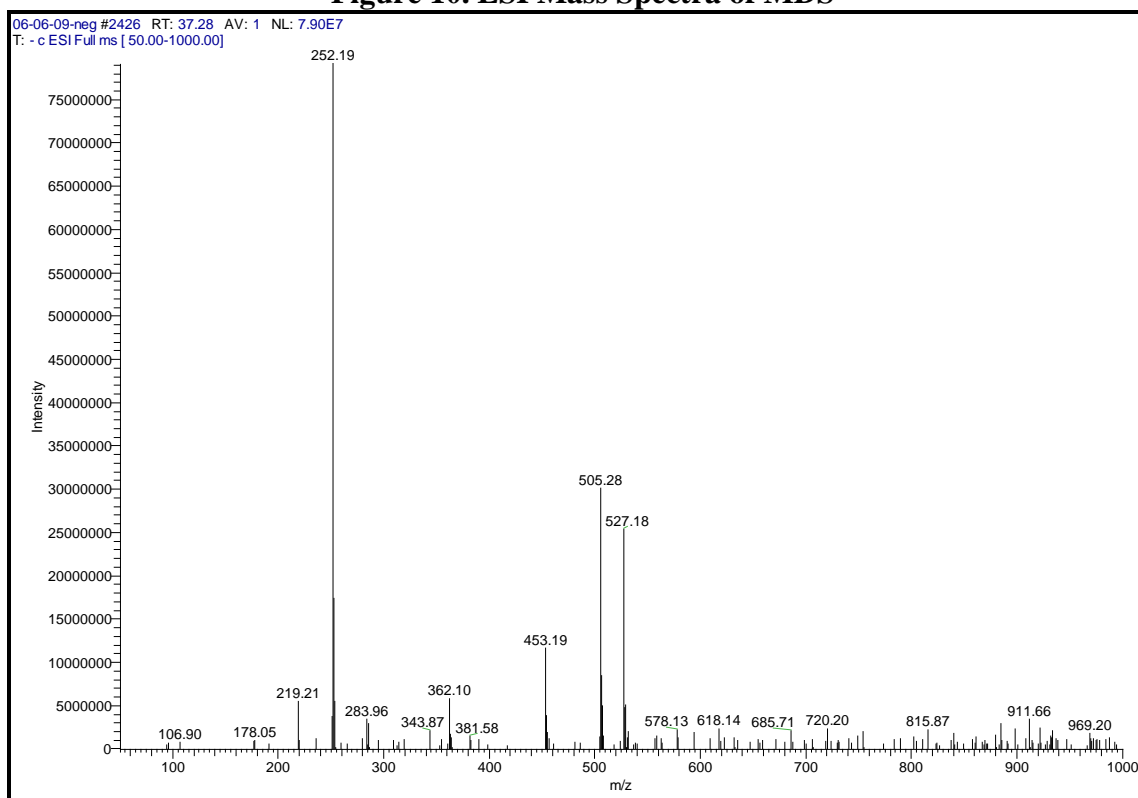**Figure 10. ESI Mass Spectra of MDS**

Figure 11 shows the ^{13}C NMR of the thiol product Mercaptodecanesulfonic acid. The carbons are labeled from 1-10 starting at the thiol and ending at the sulfonic acid. Carbon 1 peak is at 23.95 ppm, Carbon 2 at 33.04 ppm, Carbon 3 at 27.67 ppm, Carbon 4 at 28.52 ppm, Carbon 5 at 28.18 ppm, Carbon 6 at 28.37 ppm, Carbon 7 at 28.07 ppm, Carbon 8 at 23.78 ppm, Carbon 9 at 27.44 ppm, and Carbon 10 at 51.07 ppm.

Figure 11. Carbon NMR of Mercaptodecanesulfonate
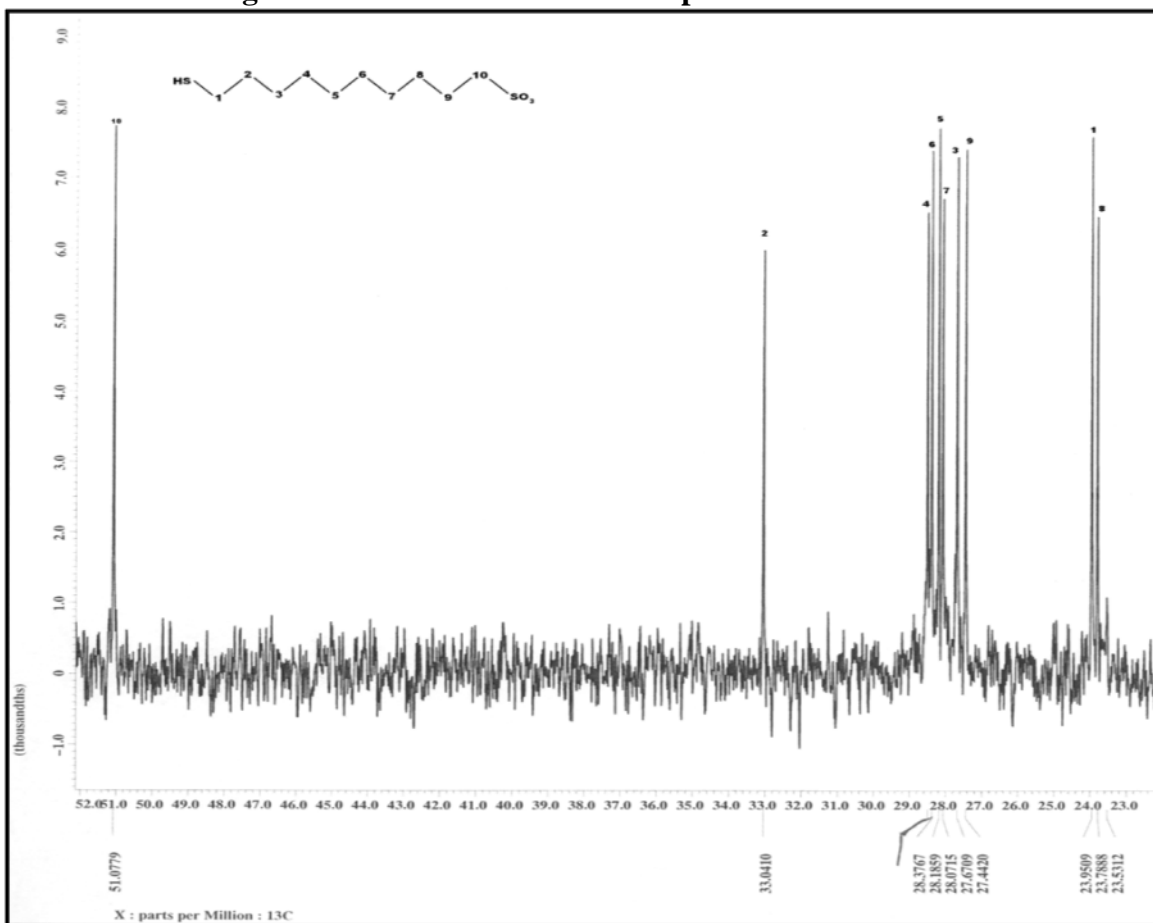
13C NMR (D$_2$O) δ 23.78 (-CH$_2$CH$_2$SO$_3$), 23.95 (SH CH$_2$-), 27.44(-CH$_2$SO$_3$), 27.67 (SH(CH$_2$)$_2$CH$_2$-), 28.07 (-CH$_2$(CH$_2$)$_3$SO$_3$), 28.18 (SH(CH$_2$)$_4$CH$_2$-), 28.37 (-CH$_2$(CH$_2$)$_4$SO$_3$), 28.53 (SH(CH$_2$)$_3$CH$_2$-), 33.04 (SHCH$_2$CH$_2$-), 51.08 (SO$_3$-CH$_2$)

Figure 12 shows the FTIR of MDS. The broad peak around 3400 cm^{-1} is most likely due to moisture in the sample. The asymmetric and symmetric methylene stretches are at 2920 and 2850 cm^{-1} respectively. The stretch from the methylene to the sulfur groups is shown at 1460 cm^{-1}. The peaks at 1184 and 1062 cm^{-1} correspond to the asymmetric and symmetric stretch between the sulfur and oxygen on the sulfonate group. The peak at 616 cm^{-1} corresponds to the carbon sulfur stretch.

Figure 12. FTIR of Mercaptodecanesulfonate
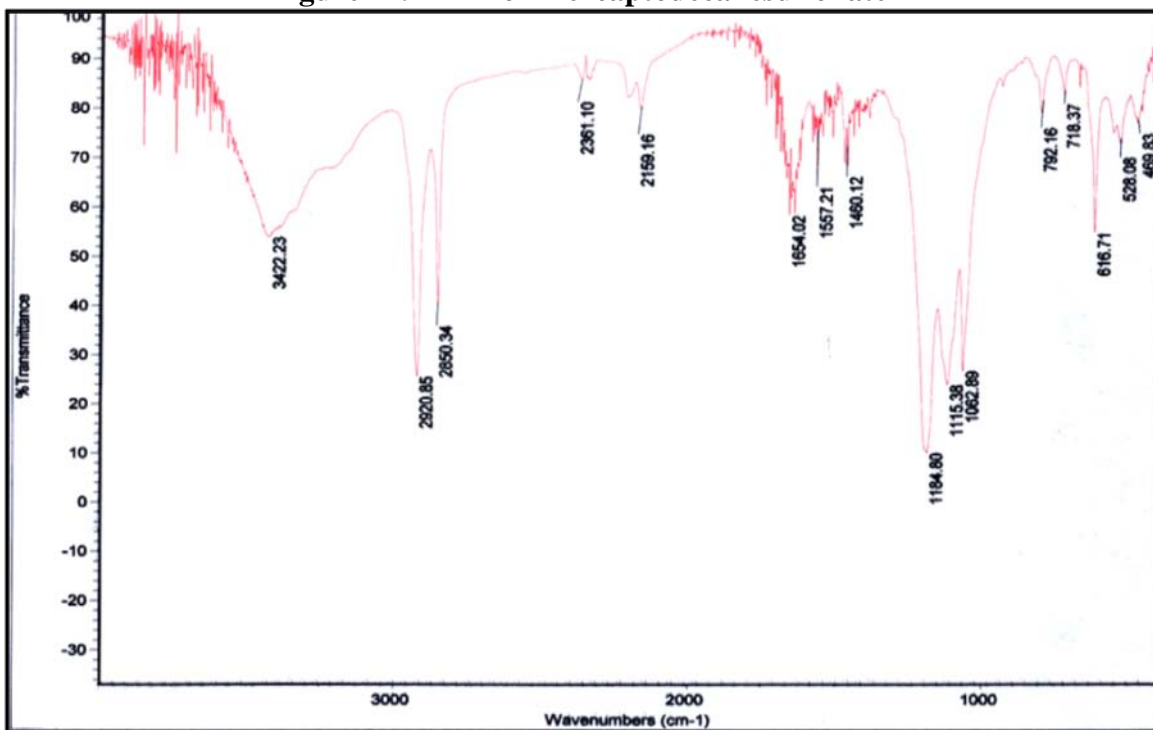
3400 cm^{-1} [moisture]; 2920 cm^{-1} [asymmetric CH$_2$ stretch]; 2850 cm^{-1} [symmetric CH$_2$ stretch]; 1460 cm^{-1} [CH$_2$-S stretch]; 1184 cm^{-1} [asymmetric S=O stretch]; 1062 cm^{-1} [symmetric S=O stretch]; 718 cm^{-1} [CH$_2$ rock]; 616 cm^{-1} [C-S stretch].

Figure 13 displays the UV-Vis absorption measurements that were used to track the 2,2'-dipyridyldisulfide exchange reaction with mercaptodecanesulfonate. As each sample was taken there was an increase in the relative absorbance signifying the release of the pyriyl-2-thione byproduct that has an absorbance around 343 nm. As the reaction came to completion the intensity of the absorbance started to level off at around 2.7 relative absorbance units.

Figure 13. UV-Vis Absorbance of MDS-pyridyldisulfide Reaction Over Time

Figure 14 shows the proton NMR that was used to characterize the disulfide product as 10-(dodecyldisulfanyl) decane-1-sulfonic acid. The triplet at around 0.8 ppm corresponds to the methyl protons. The peak from 1.2-1.4 is associated with the methylene protons. The quintuplet at 1.65 is the protons beta to the thiol and the quintuplet at 1.77 is the protons beta to the sulfonic acid. The triplet at 2.66 is the protons alpha to the thiol and the triplet at 2.7 ppm is the protons alpha to the thiol. It is important to point out that upon formation of a disulfide, the thiol peaks shift from around 2.4 further downfield to 2.66 implying that the disulfide has been formed. Also the integration of the peaks alpha and beta to the disulfide and sulfonic acid show that the disulfide peaks have roughly twice as much area since there are two of them.

Figure 14. Proton NMR of 10-(dodecyldisulfanyl) decane-1-sulfonic acid

1H NMR (CD$_3$OD, TMS) δ 0.89 (t, 3H, -CH$_2$CH$_2$**CH**$_3$), 1.25-1.46 (m, 30H, CH$_3$(**CH**$_2$)$_9$CH$_2$CH$_2$S-SCH$_2$CH$_2$(**CH**$_2$)$_6$CH$_2$CH$_2$SO$_3$), 1.67 (m, 4H, -**CH**$_2$CH$_2$S-SCH$_2$**CH**$_2$-), 1.77 (m, 2H, -**CH**$_2$CH$_2$SO$_3$), 2.67 (t, 4H, -CH$_2$**CH**$_2$S-S**CH**$_2$CH$_2$-), 2.77 (t, 2H, -CH$_2$**CH**$_2$SO$_3$)
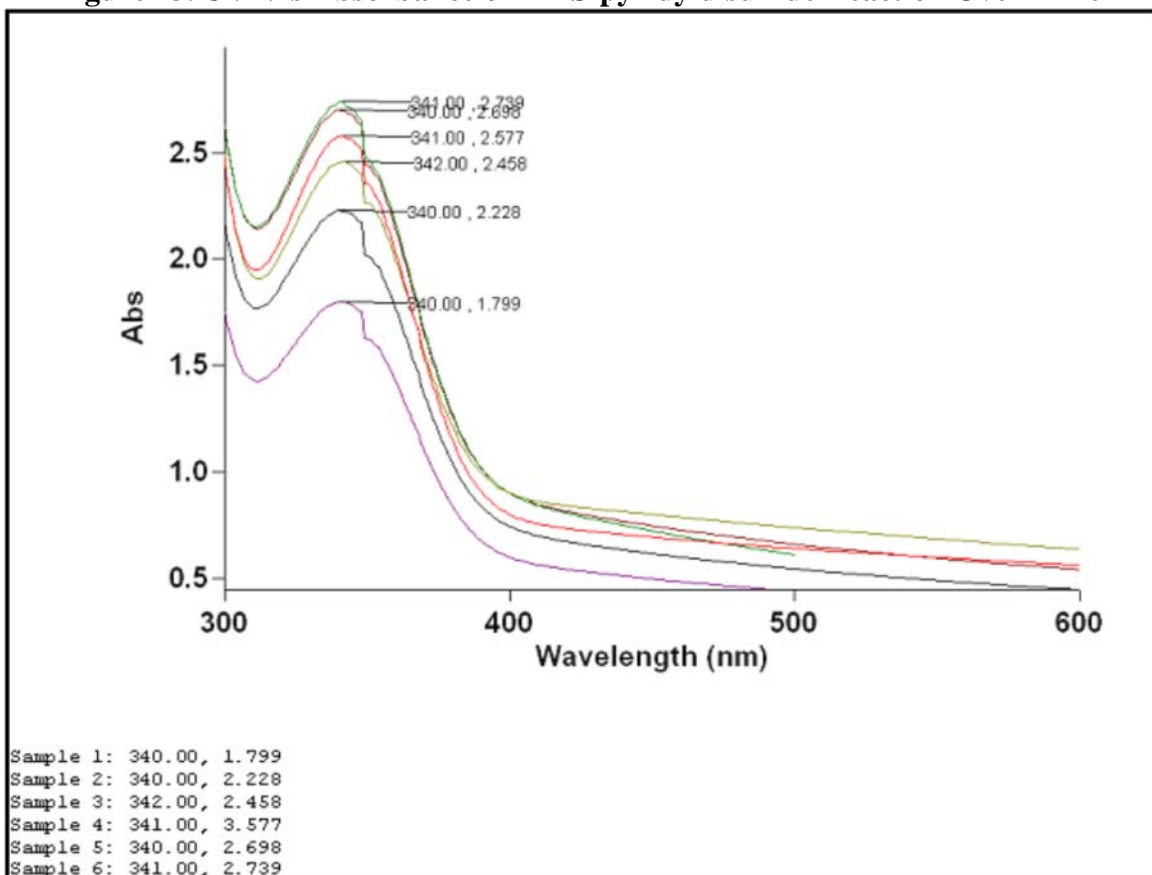
Figure 15 shows the FTIR of the asymmetric disulfide 10-(dodecyldisulfanyl) decane-1-sulfonic acid. The broad peak around 3400 is due to moisture in the sample. The asymmetric and symmetric CH_2 stretches, at 2919 and 2849 cm^{-1} respectively, have increased in intensity when compared to the thiol that was synthesized previously. This is expected due to the added methylenes from the dodecyl portion of the disulfide. The peak at 1470 cm^{-1} corresponds to the CH_2-S stretch from the disulfide and sulfonic acid. The asymmetric and symmetric S=O stretches are shown at 1168 and 1061 cm^{-1} respectively. The CH_3 deformation is shown at 1219 cm^{-1}. The C-S stretch and S-S stretches are shown at 614 and 524 cm^{-1} respectively.

Figure 15. FTIR of 10-(dodecyldisulfanyl) decane-1-sulfonic acid
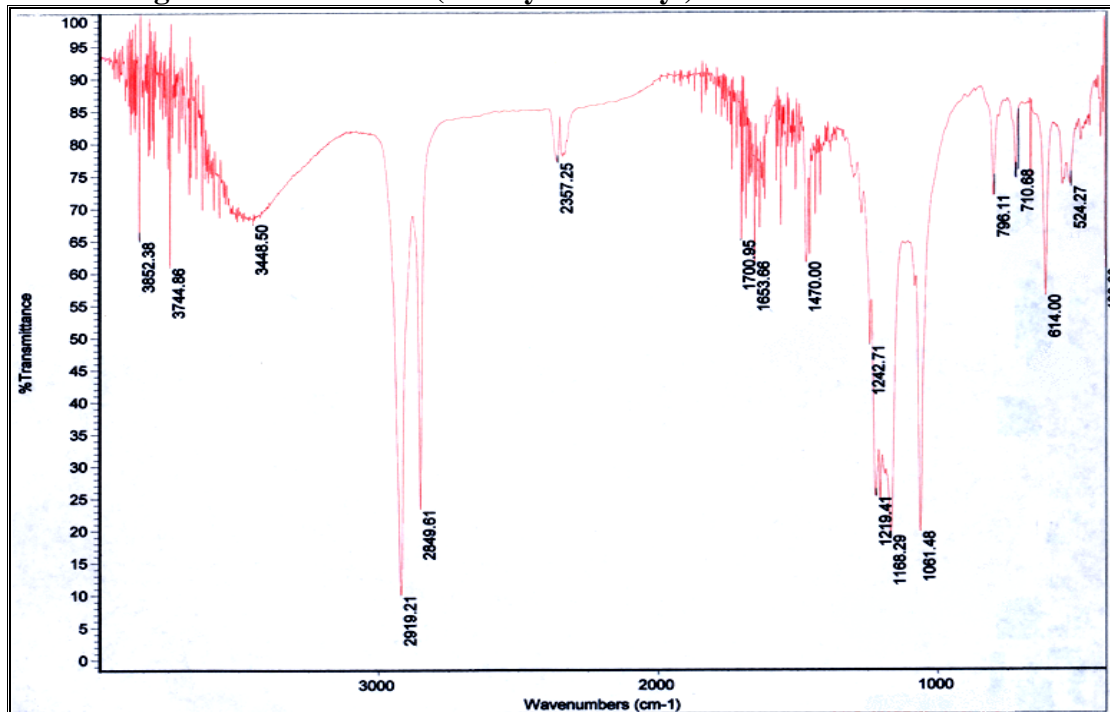
3400 cm^{-1} [moisture]; 2919 cm^{-1} [asymmetric CH_2 stretch]; 2849 cm^{-1} [symmetric CH_2 stretch]; 1470 cm^{-1} [CH_2-S stretch]; 1219 cm^{-1} [CH_3 deformation]; 1168 cm^{-1} [asymmetric S=O stretch]; 1061 cm^{-1} [symmetric S=O stretch]; 614 cm^{-1} [C-S stretch]; 524 cm^{-1} [S-S stretch]

Conclusion

The synthesis of initially the thiol mercaptodecanesulfonate and ultimately the desired disulfide, 10-(dodecyldisulfanyl) decane-1-sulfonic acid, was achieved and verified by NMR and FTIR analysis. The synthesis of the asymmetric disulfide was made possible through the use of a thiol-disulfide exchange reagent, 2,2'-dipyridyldisulfide.

CHAPTER IV

DERIVATIZATION OF GOLD NANOPARTICLES

Introduction

The next step in the project involved the production of the pseudostationary phase

to be used as the means of separation of the amyloid beta peptides. Assembly of this

pseudostationary phase required the chemisorption of 10-(dodecyldisulfanyl) decane-1-

sulfonic acid onto 10 nm gold nanoparticles. The chemisorption of disulfides onto gold

surfaces provides an ordered monolayer of the arms of the disulfide on the surface. The

use of bifunctional disulfides allows for control over the functional properties of the

monolayer.[50] Characterization of the monolayer can be performed using NMR

spectroscopy and FTIR spectroscopy. The degree of adsorption of the disulfide on the

gold surface can be followed by tracking the UV maxima of the plasmon band. A

solution of the 10-(dodecyldisulfanyl) decane-1-sulfonic acid was mixed with the citrate

stabilized nanoparticles and the degree of adsorption was detected through the shift in the

plasmon band. A proposed schematic of the functionalized nanoparticle is shown in

Figure 16. Conditions such as the time of derivatization and the concentration of the

disulfide were optimized for maximum coverage of the particles while still maintaining

particle stability in solution.

Figure 16. 10-(dodecyldisulfanyl) decane-1-sulfonic acid Functionalized Gold Nanoparticles
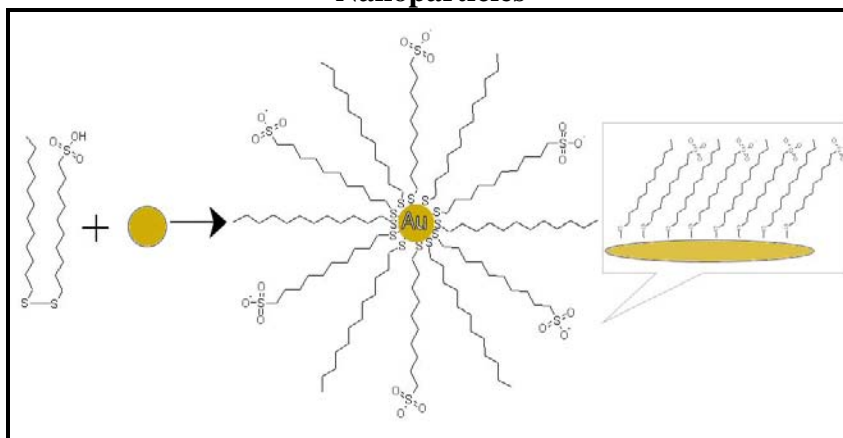
Prior to these experiments, carboxylic acid functionalized nanoparticles were synthesized that had some solubility issues in the aqueous medium. The sulfonic acid terminated nanoparticles seemed be more stable in the aqueous buffers required for the electrophoretic analysis because they stayed in solution for a longer period of time.

Materials and Methods

The chemicals used in the nanoparticle derivatization were obtained from the following companies: Acros Organics (dodecanethiol); Fisher Scientific (tetrahydrofuran); Sigma (10 nM gold nanoparticles). The mercaptodecanesulfonate and 10-(dodecyldisulfanyl) decane-1-sulfonic acid were synthesized in house.

Because of gold's affinity for sulfur containing compounds, the functionalization of gold nanoparticles is relatively straight forward. Thiols or disulfides will readily form thiolate bonds with the gold surface creating a self-assembled monolayer upon mixing a solution of the organosulfur compound with the colloidal suspension of nanoparticles. The first test was to see what concentration of disulfide would be optimal to promote self
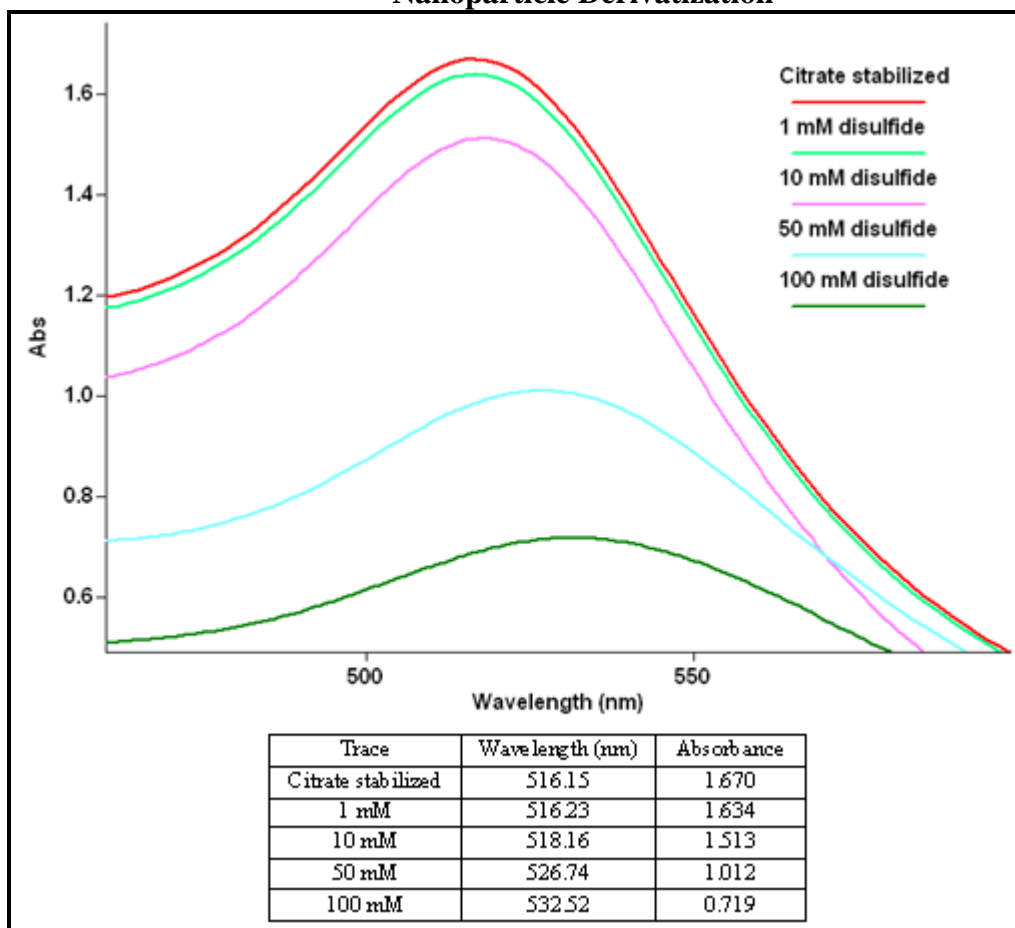
assembly of the monolayer while still maintaining particle suspension. This can be achieved by tracking the surface plasmon band using an absorption spectrophotometer. The normal maxima for the plasmon band of 10 nm gold nanoparticles is 520 nm. Upon the chemisorption of the disulfides, this plasmon band exhibits a shift to longer wavelength (~530 nm). This shift in the wavelength is due to the increase in the relative size of the particle as well as a change in the refractive index at the metal surface. The greater number of thiols that adsorb onto the surface, the greater the shift will be. This would appear as a decrease in the relative absorbance of the plasmon band. To achieve functionalization of the nanoparticles, the visible absorption spectra of 2 mL of 10 nm citrate stabilized gold nanoparticles were measured using a Cary 100 Bio UV-Visible Spectrophotometer by Varian. A 200 µL volume of a range of concentrations of the disulfide (1 mM, 10 mM, 50 mM, and 100 mM in water) were then added to the nanoparticles and vortexed vigorously. The mixture was then allowed to sit at room temperature for two hours. After that time the plasmon band maxima was once again measured. To determine the optimal derivatization time 200 µL of 10 mM disulfide was added to 2 mL of citrate stabilized 10 nm gold nanoparticles and the localized surface plasmon band was measured over time from 1 hr to 24 hr. With the optimized disulfide concentration and derivatization time, the functionalized nanoparticles were then spun down using a Savant refrigerated microcentrifuge at 13000 g for 60 minutes. The supernatant was then drawn off leaving the nanoparticle pellet. The pellet was then dried and analyzed by FTIR using the diffuse reflectance attachment. Once the derivatization was complete, the nanoparticles were centrifuged at 13000 g for 60 minutes, the

supernatant was removed and the particles were redissolved in the appropriate run buffer for use in the capillary electrophoresis experiments.

Results

In order to determine the concentration dependence of the disulfide in the functionalization of the 10 nm gold nanoparticles, the reaction was allowed to take place using a range of concentrations. The surface plasmon band was tracked over the range of derivatization conditions and as shown in Figure 17. The 1 mM disulfide solution didn't appear to shift the plasmon band from that of the citrate stabilized particles. The 10 mM solution exhibited a red shift of roughly 2 nm in the wavelength. This is consistent with the increase in particle size due to the adsorption of the disulfide onto the gold surface. The decrease in the intensity could be due to increased particle aggregation after functionalization. The higher concentrations showed a greater increase in the plasmon band maxima, but at the cost of increased aggregation. Based on these results it was determined that 200 µL of a 10 mM solution of the disulfide mixed with 2.0 mL of 5.7 x 10^{-12} particles/cm^3 of 10 nm gold nanoparticles provides the optimum tradeoff between functionalization and particle stability.

Figure 17. Effects of 10-(dodecyldisulfanyl) decane-1-sulfonic acid concentration on Nanoparticle Derivatization

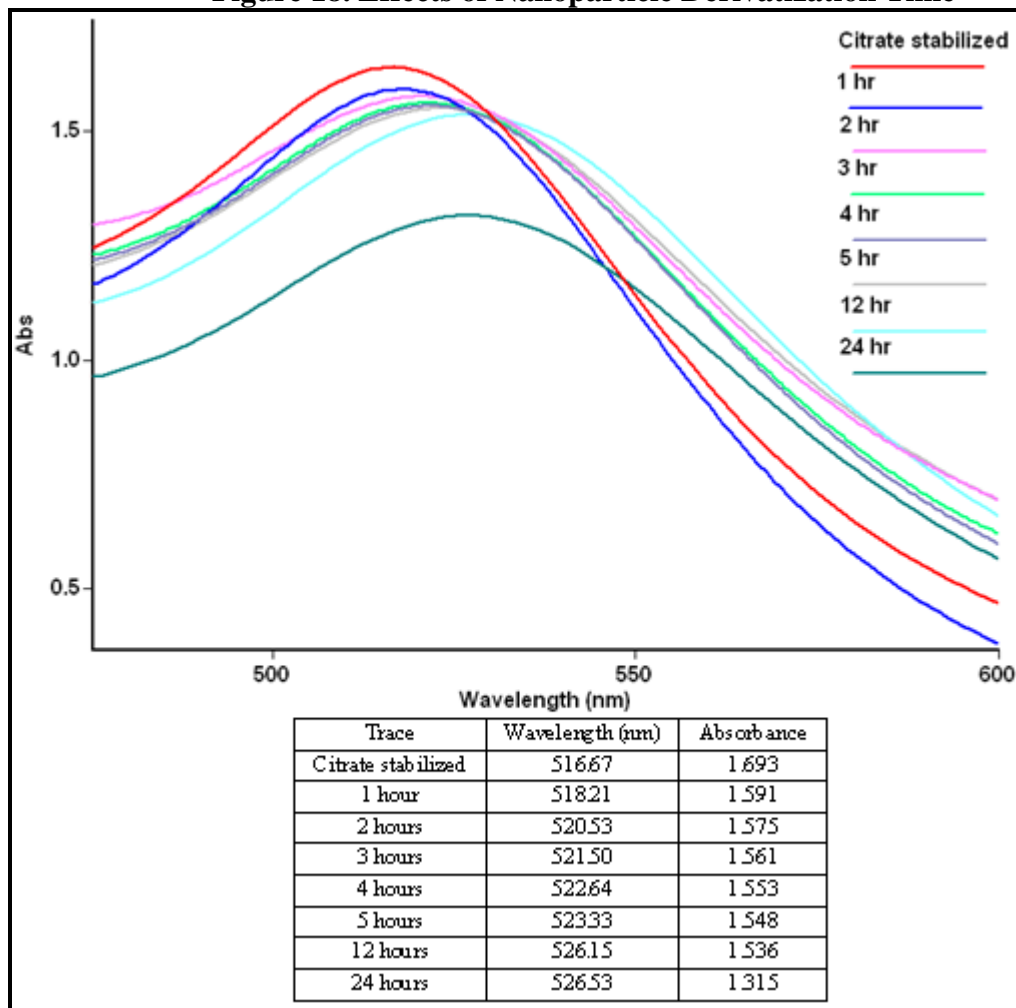| Trace	Wavelength (nm)	Absorbance
Citrate stabilized	516.15	1.670
1 mM	516.23	1.634
10 mM	518.16	1.513
50 mM	526.74	1.012
100 mM	532.52	0.719

The optimal derivatization time was determined by tracking the red shift in the maxima of the localized surface plasmon band over time. The results are displayed in Figure 18. This spectrum shows that hour by hour the plasmon band red shifts to longer wavelength. After 12 hours of derivatization the maxima had shifted from 516 nm to 526 nm. After that the maxima did not shift much farther but the intensity began to decrease most likely because of destabilization of the particles. This result implies that roughly 12

hours of derivatization time is optimal for functionalizing the nanoparticles with this

particular disulfide.

Figure 18. Effects of Nanoparticle Derivatization Time

Trace	Wavelength (nm)	Absorbance
Citrate stabilized	516.67	1.693
1 hour	518.21	1.591
2 hours	520.53	1.575
3 hours	521.50	1.561
4 hours	522.64	1.553
5 hours	523.33	1.548
12 hours	526.15	1.536
24 hours	526.53	1.315

Conclusion

The chemisorption of the previously synthesized asymmetric disulfide onto 10 nm

gold nanoparticles was realized. The conditions for the functionalization of the

nanoparticles were optimized for the concentration of the disulfide required and for the

length of the derivatization. The conditions for the derivatization reaction were optimized by tracking the effect that they had on the localized surface plasmon band. Increased adsorption leads to a red shift in the plasmon band caused by the increase in the particle size. It was discovered that a 10 mM solution of disulfide when mixed with the gold nanoparticles provides the best particle coverage with little effect on the colloidal stability. A 12 hour reaction time was shown to allow for the largest shift in the plasmon band with minimal change in the particles' ability to stay in solution.

CHAPTER V

DERIVATIZATION OF BIOMARKERS

Introduction

The biomarkers themselves do not exhibit enough native fluorescence for

quantitative measurement. This implies that in order to use laser-induced fluorescence as

the CE detection method, the peptides/proteins must be derivatized with a fluorophore.

Perhaps the more common derivatizing dyes are those that are amine reactive. In

proteins they would react with uncharged primary amines such as the N-terminus and

lysine side chains at a pH greater than their pKa. One of two probes that were used in the

amine derivatization of the amyloid beta peptides either the DyLight^{TM} dye that has an

NHS ester moiety or ATTO-TAG^{TM} FQ. The amyloid beta peptides have two residues

and an N-terminus giving them three possible reactive sites for an amine reactive probe.

As mentioned previously, the availability of multiple derivatization sites gives a

distribution of the number of attached probes. This also means that the various degrees

of derivatization will each have a different electrophoretic mobility, leading to multiple

peaks for the same analyte. Management of the pH during the derivatization can give

priority of attachment to the N-terminus over that of the side chains. The pKa of the

lysine side chain is close to 10.5 where the pKa of the N-terminus is close to 7.8. By

conducting the derivatization closer to the pKa of the N-terminus, it was thought that the

peptides would be more selectively labeled at the N-terminus. The optimal pH for the

derivatization was determined by conducting the derivatization at various pH's and

determined the number of probes attached by using MALDI-MS. The MALDI-MS

spectra of the derivatized peptides were compared to the spectra of an underivatized

sample to determine the number of attached probes. The Tau proteins were derivatized

using a thiol reactive probe. This allows for better selectivity of the probe attachment as

well as better resolution during the electrophoretic analysis because there is only one

available derivatization site, cysteine, on the protein. This implies that the single

derivatization site would lead to a single detectable peak. The conditions of this

derivatization were based on the literature from the dye manufacturer. The derivatized

Tau protein was also analyzed by MALDI-MS and compared to the spectra of an

underivatized sample to ensure the attachment of a single probe per protein.

Materials and Methods

The materials used in this project were obtained from the following companies:

Acros Organics (CAPS, dimethylformamide, MES, potassium cyanide, trifluoro acetic

acid); Fisher Scientific (acetonitrile, ammonium hydroxide, potassium phosphate

monobasic); GE Healthcare (10 K spin filter, 30 K spin filter); Molecular Probes (ATTO-

TAG^{TM} FQ); Pharmco AAPER (methanol); rPeptide (Amyloid Beta 1-40, Amyloid Beta

1-42, Human Tau-352); Sigma Aldrich (α-cyano-4-hydroxycinnamic acid, dimethyl

sulfoxide, sodium tetraborate); Thermo Scientific (DyLight^{TM} 488 NHS Ester, DyLight^{TM}

488 Maleimide).

The Tau protein fluorescent derivatization was achieved using a thiol reactive dye

(DyLight^{TM} 488 Maleimide) because the protein has a single cysteine allowing for a

single derivatization. Upon receipt, 100 µg of Human Tau-352 was reconstituted in 100

µg of nanopure water to give a protein concentration of 1 mg/mL in 50 mM MES buffer

at pH 6.8, 100 mM sodium chloride, and 0.5 mM EDTA. The DyLight^{TM} 488 maleimide

(1 mg) was dissolved in 100 µL of dimethylformamide (DMF). Then 20 µL of the dye

were added to the 100 µL of peptide and vortexed. The derivatization reaction was then

allowed to proceed overnight (~10 hr.) The non reacted dye was removed by adding the

mixture to a 30 kDa molecular weight cutoff spin filter for 30 minutes at 9000 g. The

filtrand was then washed 3 times with 100 µL portions of 10 mM sodium borate at pH

10.0. The resulting filtrand was reconstituted in 100 µL of 10 mM sodium borate at pH

10.0. The 100 µL of derivatized Tau at a concentration of 27 µM was divided into 20

single use fractions of 5 µL. These were then dried using a Savant Speed Vac (SC110)

with no heating and stored at -20˚C for later use.

The amyloid beta peptides (1 mg $A\beta_{40}$ and 1 mg $A\beta_{42}$) were originally

reconstituted in 1 mL of 1% ammonium hydroxide to give the peptides at a concentration

of 1 mg/mL (231 µM $A\beta_{40}$ and 222 µM $A\beta_{42}$). Once they were dissolved they were

sonicated for 30 seconds to 1 minute. These solutions were either used directly in the

derivatization with the DyLight^{TM} 488 NHS ester or they were separated into 20 µL

fractions for later derivatization with ATTO-TAG^{TM} FQ. The 20 µL $A\beta_{40}$ fractions were

diluted with 23.1 µL of 18.65 mM sodium tetraborate at pH 10 to give 200 µM $A\beta_{40}$ in

10 mM sodium tetraborate at pH 10. The 20 µL fractions of $A\beta_{42}$ were diluted with 22.2

µL of 10 mM sodium tetraborate at pH 10 to give 200 µM $A\beta_{42}$ in 10 mM sodium

tetraborate at pH 10. These fractions were then stored at -20˚C for later use.

To derivatize the amyloid beta peptides with the DyLight^{TM} amine reactive dye,

the 1 mL of peptide was diluted with 100 µL of 550 mM Borate. This gave the peptide in

0.05 M sodium borate buffer at pH 8.5. Then 100 µL of either $A\beta_{40}$ or $A\beta_{42}$ were added to the vial containing 50 µg of the dye. The resulting solution was mixed well and incubated at room temperature for 1 hour. The excess dye was then removed using a 3 kDa cutoff spin filter. The filtrand was rinsed three times with 200 µL portions of 10 mM sodium tetraborate then reconstituted with 1 mL of 10 mM sodium tetraborate buffer at pH 10. The derivatized peptides were then separated into 40 µL aliquots and dried by speed vacuum with no heat. The aliquots were stored at -20˚C for later use.

For derivatization of the amyloid beta peptides with ATTO-TAG^{TM} FQ, a 10 mM solution of the ATTO-TAG^{TM} FQ was prepared by dissolving 10 mg of FQ in 4.0 mL of methanol. The dye solutions were then divided up into 10 µL aliquots, dried using a speed vacuum, and stored at -20˚C until later use. The derivatization buffer was prepared by dissolving potassium cyanide in 10 mM borate buffer at pH 10 to give 10 mM KCN. When required for derivatization, an aliquot of the dye was redissolved in 10 µL of methanol to give 10 mM dye. Then 20 µL of the derivatization buffer was added to 4 µL of the peptide. The 10 µL of dye was then added to the peptide solution, the solution was mixed, and allowed to sit at room temperature for 1 hour. After one hour the solutions were diluted to give the desired concentration of peptide using the appropriate concentration of run buffer so that the final concentration of buffer in the sample was 1/10 of what the background electrolyte in the CE experiment was going to be.
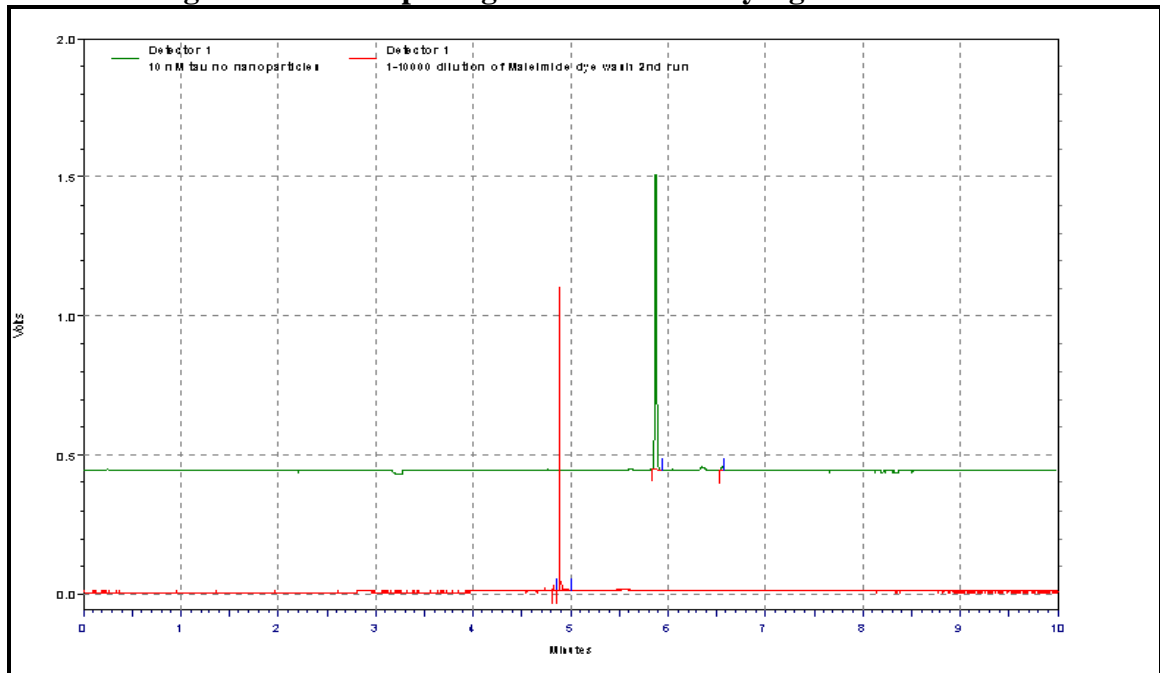
In order to determine the pH dependence of the derivatization, the above procedure was carried out using 10 mM sodium tetraborate buffer at pH 7.0, 7.5, 8.0, 8.5,

9.0, 9.5, 10.0, 10.5, and 11.0. After the one hour derivatization time the samples were diluted with nanopure water to give the peptides at 25 µM. The MALDI matrix that was chosen was α-cyano-4-hydroxycinnamic acid, which was prepared by dissolving 8 mg in 1 mL of matrix diluent (50 % acetonitrile, 0.1% trifluoro acetic acid in water). The matrix was vortexed vigorously for 30 seconds and centrifuged at 1000 g for 2 minutes. To prepare the samples for spotting, 1 µL of the peptide was mixed with 12 µL of matrix diluent, and 12 µL of the supernatant from the centrifuged matrix solution to give the peptide samples at 1 µM on the plate. From these solutions, 0.5 µL were spotted onto a clean and dry MALDI plate and the spots were allowed to dry for subsequent analysis on an Applied Biosystems 4700 MALDI-TOF.

Results

For the tau protein, probe attachment was verified by electrophoretic analysis. Multiple analyses on both the filtrand and the filtrate of the tau derivatization showed that the filtrand (protein) had a different electrophoretic mobility than the filtrate (excess dye). Both the filtrate and filtrand diluted so that the sample buffer concentration was 4 mM borate at pH 10. They were then hydrodynamically injected into a 67 cm capillary with an inner diameter of 50 µm. The voltage for this analysis was set to 25 kV. This result is shown in Figure 19 with the protein (green trace) having an elution time of 5.8 minutes and the dye (red trace) eluting at 4.8 minutes. Note that the mobilities differ by roughly one minute and there is no trace of the excess dye appearing in the tau analysis. The electropherogram for the filtrate (excess dye) was verified to be the DyLight[TM] maleimide through a subsequent analysis of the pure dye (not shown) where the electrophoretic peak of the pure dye aligned with the peak for the filtrand at 4.8 minutes.

Figure 19. Electropherogram of Tau and DyLight™Maleimide

In order to determine the pH dependence of the derivatization of the amyloid beta peptides with ATTO-TAG™ FQ, multiple derivatizations were conducted where the only variable was the pH of the derivatization buffer which varied every 0.5 pH units from 7.0 to 11.0. After derivatization the samples were mixed with MALDI matrix as described above and spotted onto a MALDI plate for analysis by mass spectrometry. Since there are three possible derivatization sites on the amyloid beta peptides (N-terminus and two lysine side chains), it was expected that there would be distribution of masses corresponding to the attachment of 0-3 molecules of FQ. The reaction of ATTO-TAG™ FQ with an uncharged primary amine is displayed in Figure 20. The attachment of the

Figure 20. ATTO-TAG FQ Reaction

ATTO-TAG FQ™ + R-NH₂ + CN⁻ → Cyanoisoindole derivative
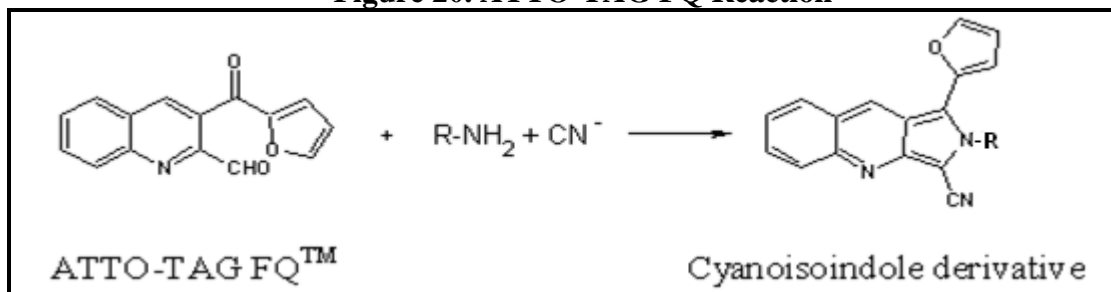
tag to the protein or peptide results in a mass difference of approximately 242 g/mol. On amyloid

beta 40, which has a mass of 4328.8 Da, this corresponds to masses of 4328.8 Da, 4570.8 Da,

4812.8 Da, and 5054.8 Da for the attachment of 0 probes, one probe, two probes, and three

probes respectively. For amyloid beta 42, the attachment of ATTO-TAG™ FQ corresponds to

masses of 4514.8 Da, 4756.8 Da, 4998.8 Da, and 5240.8 Da for the attachment of no probes, one

probe, two probes, and three probes respectively. When attempting to determine the molecular

weight of the amyloid beta peptides prior to and after derivatization, the signal appeared to be

weak for $A\beta_{42}$. This was contributed to increased aggregation of this longer peptide. A previous

study showed that the peptides would be in their monomeric form if they were originally

reconstituted in pure dimethylsulfoxide (DMSO) rather than 1% ammonium hydroxide.[51] From

that point the peptides were initially reconstituted in DMSO and the signal for the peptides was

much stronger. It was expected that by derivatizing the peptides at a pH that is closer to the pKa

of the N-terminus (pH=7.5) and below the pKa of the lysine side chains (pH=10.5), there would

be a more selective attachment of the probe to the N-terminus. This would appear as an increase

in the area of the peak corresponding to a single probe attachment. The results were, however,

somewhat counterintuitive. The data in Table 1 show the percentage of tags that were attached to

amyloid beta 40 and amyloid beta 42 based on a ratio of the MS peak areas. These results could

be rationalized by the pH, in some way, affecting the availability of the derivatization site for dye

attachment. The tables do, however, show that for both peptides, pH 10.5 gives the highest

ratio of a single peak which corresponds to the attachment of two dye molecules. This

implies that in an electrophoretic experiment 95% of the peptides will travel under the

Table 1. pH dependence of Amyloid Beta derivatization

Amyloid Beta 40					Amyloid Beta 42			
pH	% no probes	% 1 probe	% 2 probes	% 3 probes	pH	% no probes	% 1 probe	% 2 probes	% 3 probes
7.0	3	12	54	31	7	0	5	80	15
7.5	0	14	55	31	7.5	0	9	64	27
8.0	2	13	55	30	8	0	5	82	13
8.5	0	10	83	7	8.5	0	1	79	20
9.0	6	29	38	26	9	2	29	57	11
9.5	0	20	80	0	9.5	0	9	91	0
10.0	0	27	73	0	10	0	16	84	0
10.5	0	5	95	0	10.5	0	6	94	0
11.0	0	15	74	11	11	0	9	91	0

same peak corresponding to the peptide with two dye molecules attached. Only 5%

would travel under a separate peak relating to single dye attachment. Because this pH

gives the highest likelihood of a single electrophoretic peak, it was chosen for further

derivatizations. Figure 21 shows the MALDI mass spectra in positive linear mode for a)

underivatized $A\beta_{40}$, b) the derivatization of $A\beta_{40}$ at pH 7.0 which shows the masses of the

different extents of derivatization, and c) the derivatization of $A\beta_{40}$ at pH 10.5 which

gives mostly (~95%) the signal for two dye attachments with a smaller peak (~5%) for

the single dye attachment. Figure 22 displays the MALDI mass spectra in positive linear

mode for a) the underivatized $A\beta_{42}$, b) the derivatization of $A\beta_{42}$ at pH 9.0 which shows

the masses of the different extents of derivatization, and c) the derivatization of $A\beta_{42}$ at

pH 10.5 which shows mostly two dye attachments (~94%) and a smaller peak for a single

dye attachment (~6%).
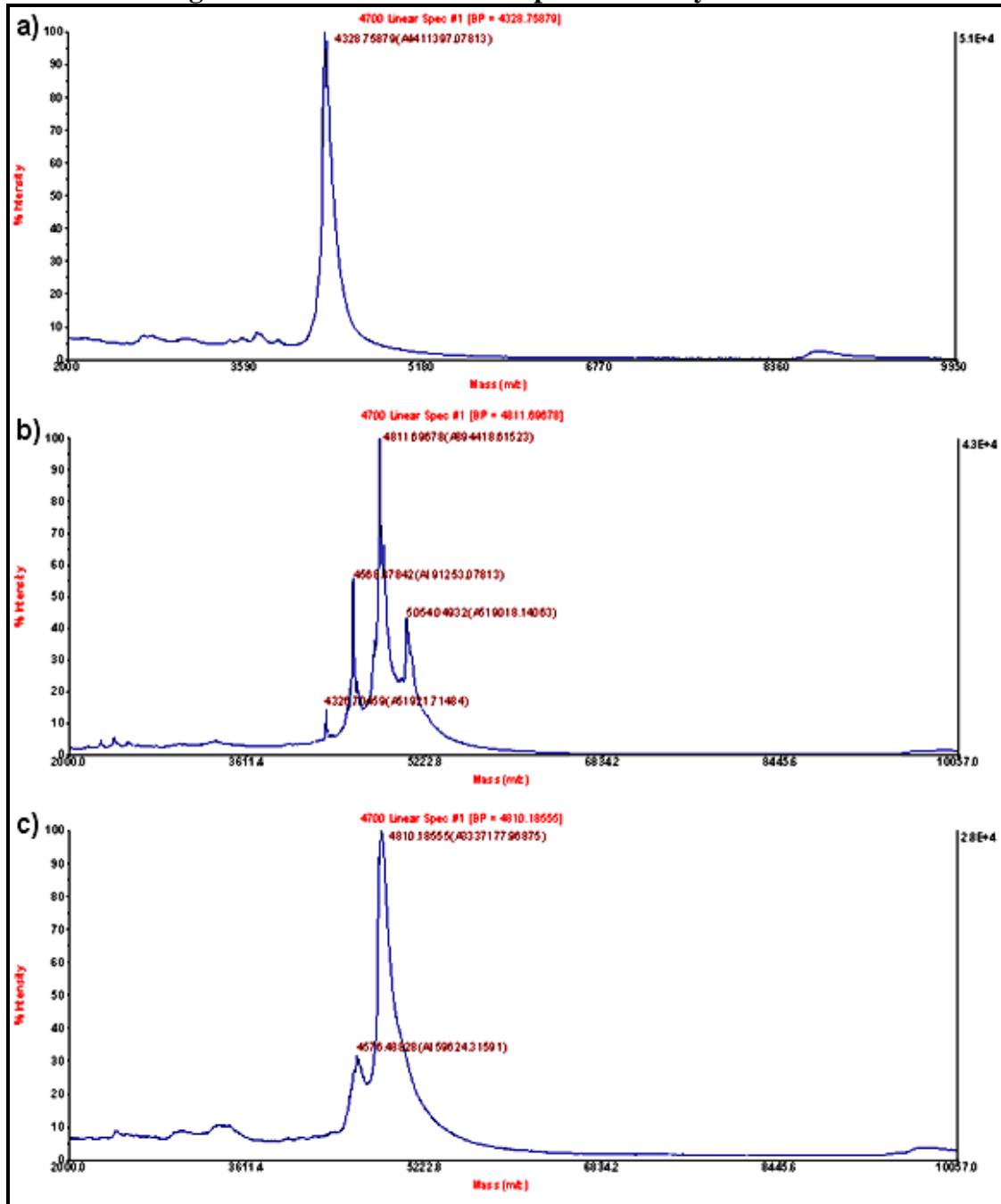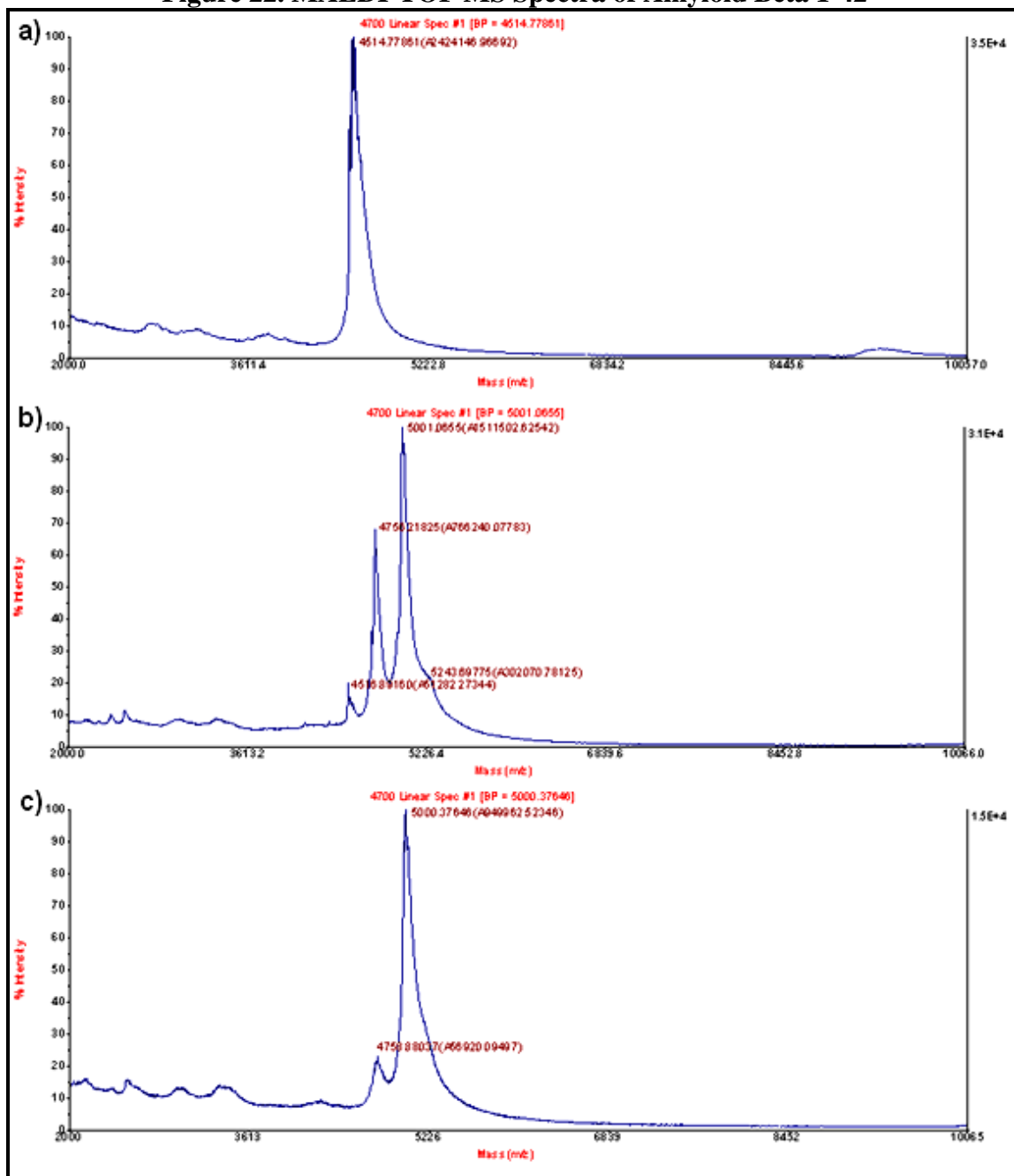
Figure 21. MALDI-TOF MS Spectra of Amyloid Beta 1-40

Figure 22. MALDI-TOF MS Spectra of Amyloid Beta 1-42

Conclusion

The derivatization of the amyloid beta peptides and tau protein were initially conducted using the appropriate DyLight^{TM} dye. This dye was sufficient for the Tau protein, however due to its large size it inhibited the separation of the amyloid beta peptides. Because of this the peptides were derivatized with a smaller dye, ATTO-TAG^{TM} FQ. The analysis of the derivatization of these peptides over a range of pH values using MALDI showed that the high pH derivatizations exhibited the highest MALDI signal as well as the most monodispersity in the molecular weights. Because of this, pH 10.5 was chosen as the optimal pH for the derivatization of the amyloid beta peptides.

CHAPTER VI

CE SEPARATION OF BIOMARKERS USING A NANOPARTICLE
PSEUDOSTATIONARY PHASE

Introduction

In this portion of the research, the nanoparticles that were functionalized with 10-

(dodecyldisulfanyl) decane-1-sulfonic acid were implemented as a pseudostationary

phase in the capillary electrophoretic analysis of the Alzheimer's Disease biomarkers.

The main goal in using the functionalized nanoparticles was to achieve separation

between the two amyloid beta peptides. The principles behind the separation are a

combination of MEKC and CEC. The nanoparticles act like the micelle pseudo

stationary phase of an MEKC experiment, but will be more stable since the stationary

phase is bonded to the particles as in CEC. On the surface of the particles are the

alternating arms of the asymmetric disulfide: a 12 carbon alkyl chain and a 10 carbon

alkyl sulfonic acid. Since the sulfonic acid is deprotonated at almost every pH, the

charge around the outside of the particle will be negative. When the electric field is

applied the nanoparticles begin to migrate towards the anode which is at the inlet. The

proteins and peptides in the sample plug have an overall positive charge and will have an

electrophoretic mobility in the direction of the cathode because of the high pH of the run

buffer and sample buffer (pH 10). Under these conditions the nanoparticles and

biomarkers are migrating in opposite directions, the interactions between the

proteins/peptides and the nanoparticles are exploited. The dodecane arms act as a site of

hydrophobic interaction and the sulfonic acid acts as an ion exchange site between the biomarkers and the nanoparticles. The nanoparticles allow for the separation of the analyte according to its partitioning into the stationary phase. The more the biomarkers interact with the nanoparticles; the closer the biomarkers' retention time will be to that of the nanoparticles. The analysis conditions were optimized for the separation and quantitation of the amyloid beta peptides and were compared to runs without the pseudo stationary phase as a proof of concept. Conditions were then optimized for the quantitation of the total tau protein with the nanoparticles. This analysis was also compared to a control run without the nanoparticles. An experiment was then conducted for the separation of a mixture of the amyloid beta peptides and the tau protein.

Materials and Methods

The chemicals that were used in this section were obtained from the following companies: Acros Organics (CAPS, MES); Fisher Scientific (sodium hydroxide); Pharmco AAPER (hydrochloric acid).

The separation of the Alzheimer's Disease biomarkers was realized using functionalized gold nanoparticles as a pseudostationary phase in a capillary electrophoretic experiment. Shown in Figure 23 is a representation of the interaction between the peptides and the nanoparticles. This figure shows three different snapshots of the capillary at different time points in the separation. Right after injection (t=0), the peptides are mixed and would be coeluting if detected at that point. After the voltage is applied the nanoparticles are going to have a large electrophoretic mobility towards the inlet because of the sulfonic acid, while the electroosmotic flow will be towards the outlet. Later on in the capillary the peptides will be selectively interacting with the particles either through hydrophobic or ion exchange interactions causing the

peaks to start to separate (t=5). By the time the peptides reach the detector in the last part of the figure they should have achieved separation (t=10).

Figure 23. Mechanism for the Separation of AB40 from AB42
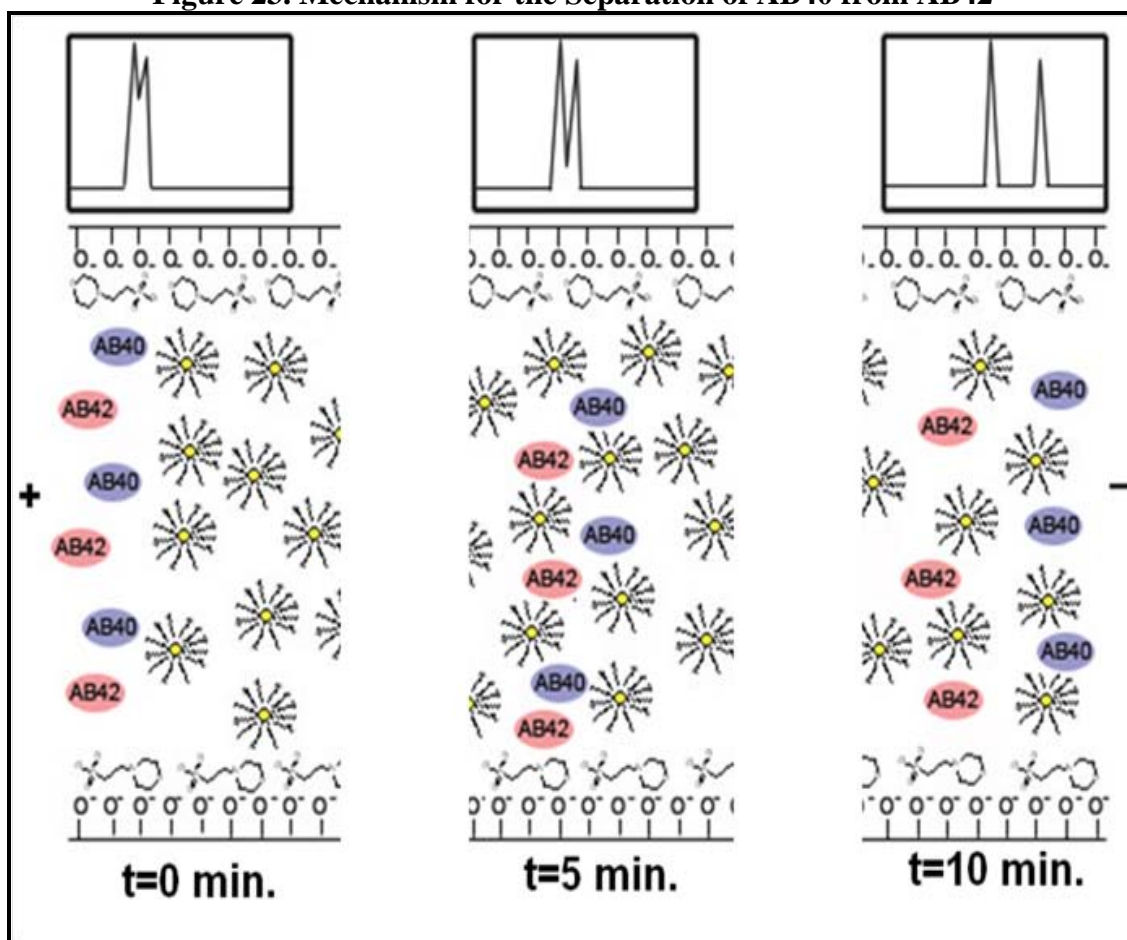
The instrumentation and parameters that are to be described were consistent throughout all of the CE analyses unless otherwise specified. The capillary had a 50 µm inner diameter and an effective length of 50 cm from inlet to detector with a total length of 67 cm from inlet to outlet. The capillary was installed in a Groton Biosystems GPA100 CE with a Picometrics Zetalif LIF-SA-03 detector. The laser used to induce the

fluorescence was a Melles Griot 43 Series Argon Ion Laser connected to the detector via optical cable. The excitation wavelength was set to 488 nm with a light controlled excitation power of 10 mW. The capillary was preconditioned upon installation by flushing the capillary with 0.2 M sodium hydroxide for 30 minutes at 1000 mbar. In between analyses the capillary was flushed with 0.1 M sodium hydroxide for 5 minutes, nanopure water for 5 minutes, and run buffer for 5 minutes each at 1000 mbar. In order to maintain retention time reproducibility the outlet vial was removed before and replaced after flushing with sodium hydroxide to keep the buffer pH consistent. Sample injections were made hydrodynamically at 100 mbar for 3 seconds. A three second injection time at this pressure gives an injection volume of 8.86 nL which corresponds to an injection plug length of 4.50 mm. The background electrolyte (BGE) was either 40 mM CAPS buffer at pH 10.0 or 40 mM MES buffer at pH 5.0. These buffers also contained functionalized nanoparticles for some analyses. The sample buffers were kept at 1/10 the concentration of the BGE in order to exhibit sample stacking.

The amyloid beta peptides and the tau protein were originally derivatized with the appropriate DyLight^{TM} dye and analyzed by capillary electrophoresis using a 40 mM CAPS buffer at pH 10.0 both with and without the 10-(dodecyldisulfanyl) decane-1-sulfonic acid functionalized nanoparticles. The potential across the capillary was initially set to 25 kV. Despite exhibiting a delayed elution time when analyzed with the functionalized nanoparticles in the buffer, the conditions were not sufficient to separate the amyloid beta peptides.

The amyloid beta peptides were then derivatized using the smaller ATTO-TAG[TM] FQ and analyzed by CE with 40 mM MES pH 5 as the background electrolyte. This same buffer was used to suspend the functionalized gold nanoparticles for runs where the pseudostationary phase was used. Since decreasing the applied voltage increases the retention time[52], the potential across the capillary was also lowered to 10 kV to allow more time for interaction between the particles and the biomarkers.

Results

The CE analysis of $A\beta_{40}$ (100 nM), $A\beta_{42}$ (100 nM), and tau protein (10 nM) each derivatized using the DyLight[TM] dye with the CAPS buffer at pH 10 showed no separation of the amyloid betas (Figure 24). Both the $A\beta_{40}$ and $A\beta_{42}$ eluted at close to 5 minutes. There is a second peak that elutes at around 6.6 minutes that has been accredited to excess dye either left over from the derivatization or that was hydrolyzed

Figure 24. Electropherogram of Tau, AB40, AB42, and mix (DyLight™) without nanoparticles
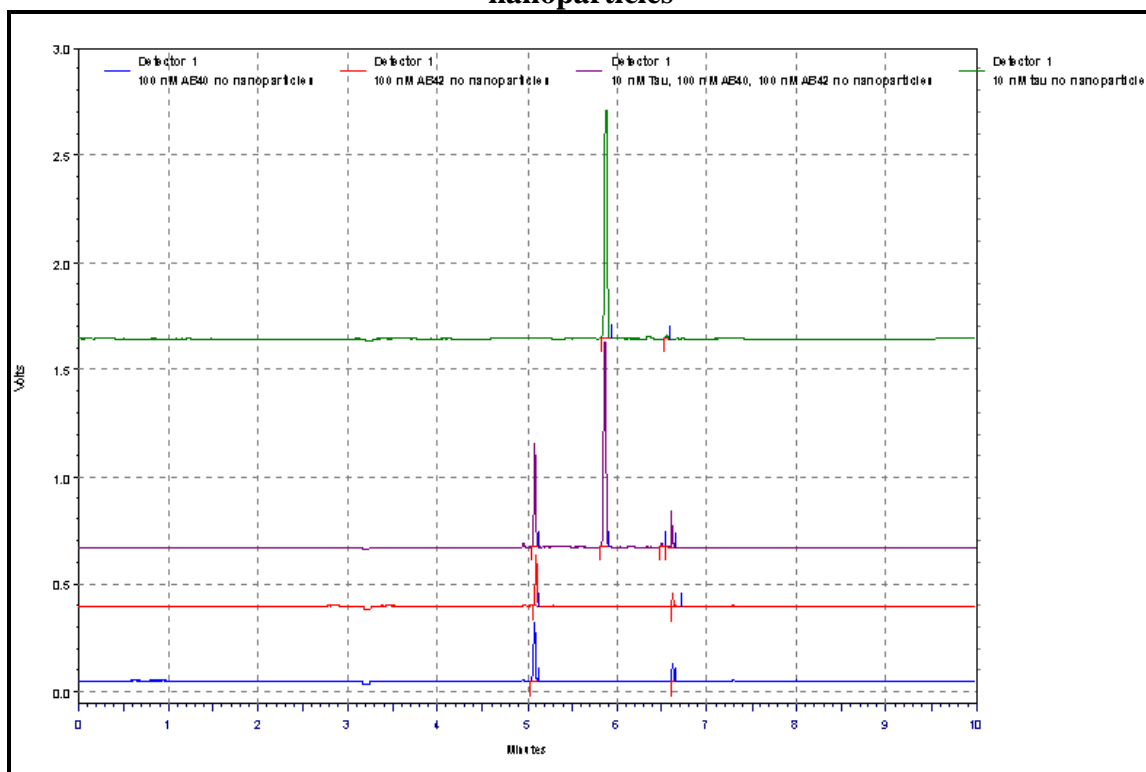
from the peptides. This conclusion was confirmed by CE analysis of the NHS ester of the dye under the same electrophoretic conditions which eluted at 6.6 minutes. It can be seen that the peak height of the peptides (5.1 minutes) is roughly doubled in the analysis of the mixture (pink trace) when compared to each of the separate analyses (blue trace for $A\beta_{40}$, red trace for $A\beta_{42}$) implying that the peptides are coeluting which is expected under these conditions. The tau protein is easily separated from the peptides and elutes at around 5.9 minutes (green trace). It also doesn't appear to effect the migration time of the peptides.

Under the same conditions as above, the analysis was repeated, only this time the run buffer contained the functionalized gold nanoparticles. As shown in Figure 25, the elution times have been shifted to later times, by a little over a minute. This shift in the elution time can be attributed due to the interaction of the peptides and protein with the gold nanoparticles. Despite the interaction with the nanoparticles, there is no clear separation between $A\beta_{40}$ and $A\beta_{42}$. This could be due to the fact that the dye molecule is rather large (1000 Da), which might negate the small difference in the peptides' mass to charge ratios and the slight differences in their polarities.

Figure 25. Electropherogram of Tau, AB40, AB42, and mix (DyLight™) with functionalized nanoparticles
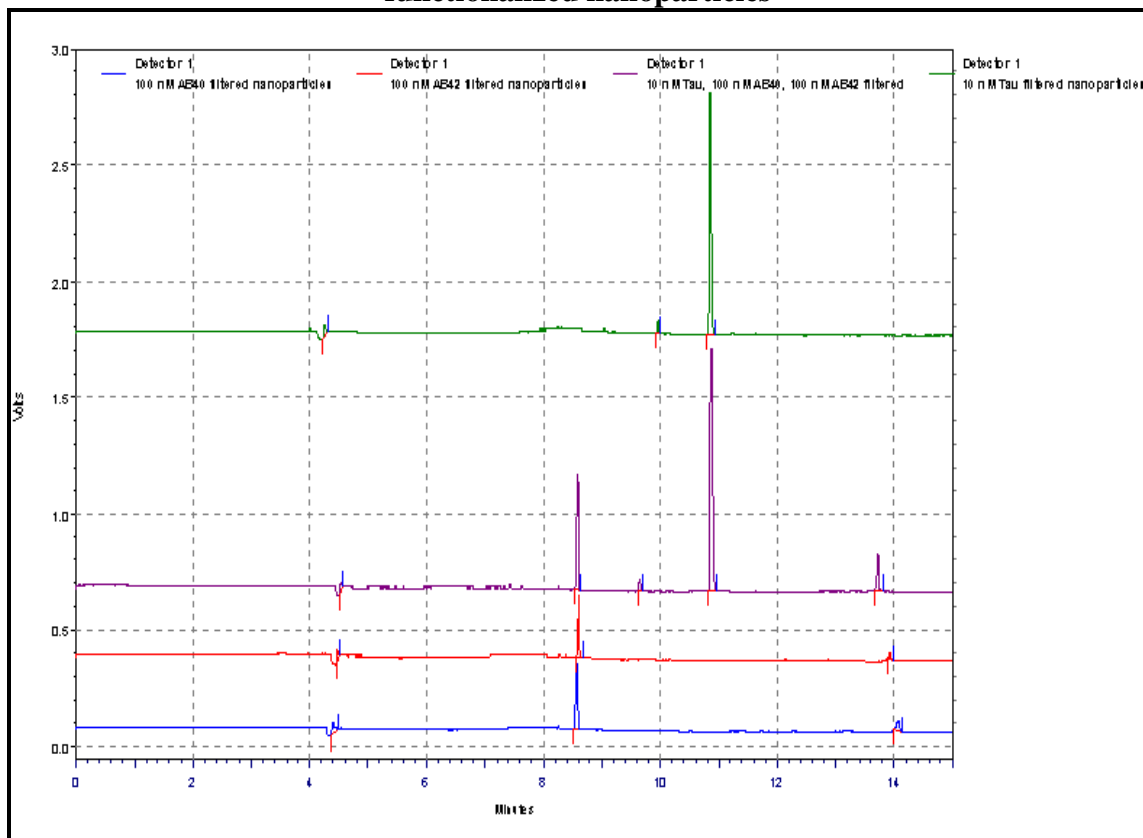
Figure 26 Figure 28 shows a comparison of the electropherograms of 100 nM $A\beta_{40}$ with and without nanoparticles. The bottom blue trace shows the electropherogram of $A\beta_{40}$ in the analysis that did not contain nanoparticles in the run buffer. The peptide is shown eluting at approximately 5 minutes with the free dye around 6.75 minutes. The top red trace shows the electropherogram of $A\beta_{40}$ in the analysis that had nanoparticles in the run buffer. The peptide's retention time was shifted to approximately 8.5 minutes.

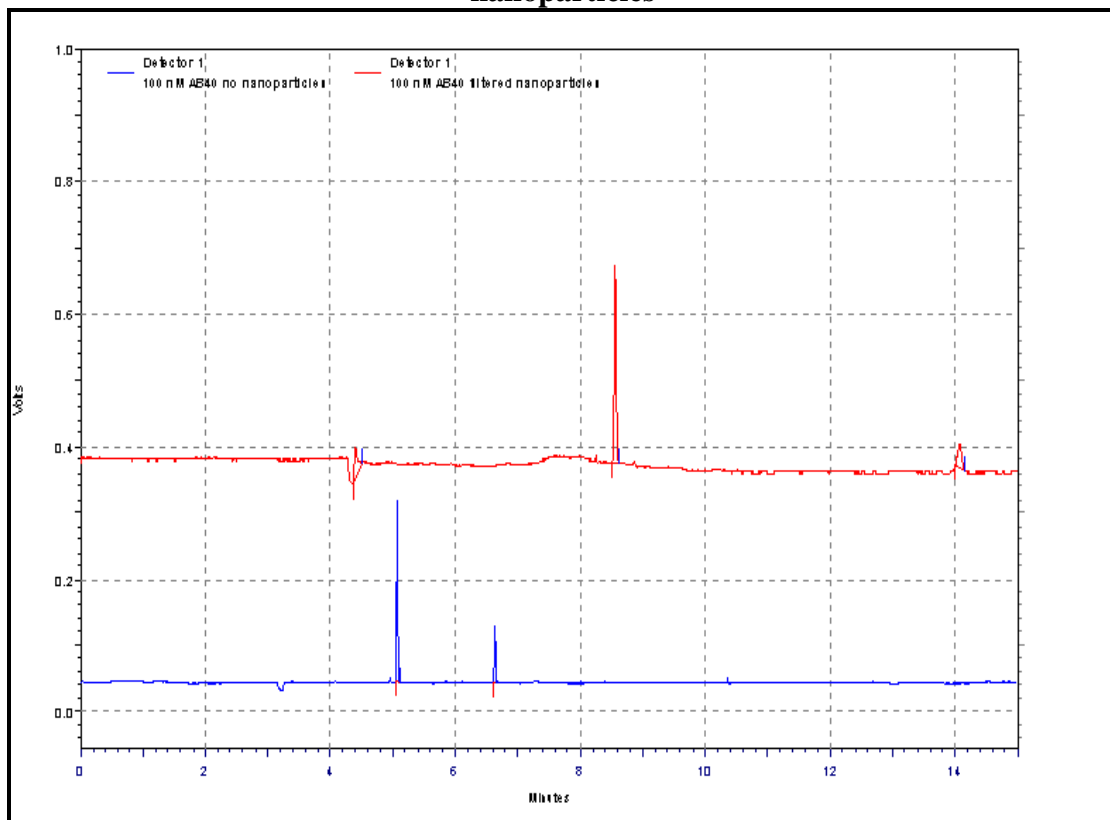**Figure 26. Electropherogram of AB40 (DyLight™) with/without functionalized nanoparticles**

Figure 27 shows the comparison in the electropherograms of $A\beta_{42}$ both with and without nanoparticles to demonstrate the effect that the nanoparticles have on the retention time of the peptide. The bottom blue trace shows 100 nM $A\beta_{42}$ in the analysis that did not have the functionalized nanoparticles in the run buffer. The peptide is shown eluting after 5 minutes with the free dye eluting at 6.75 minutes. The top red trace shows $A\beta_{40}$ in the analysis that did contain the nanoparticles in the run buffer demonstrating a shift in the elution time of the peptide to 8.5 minutes and the free dye to about 14 minutes.

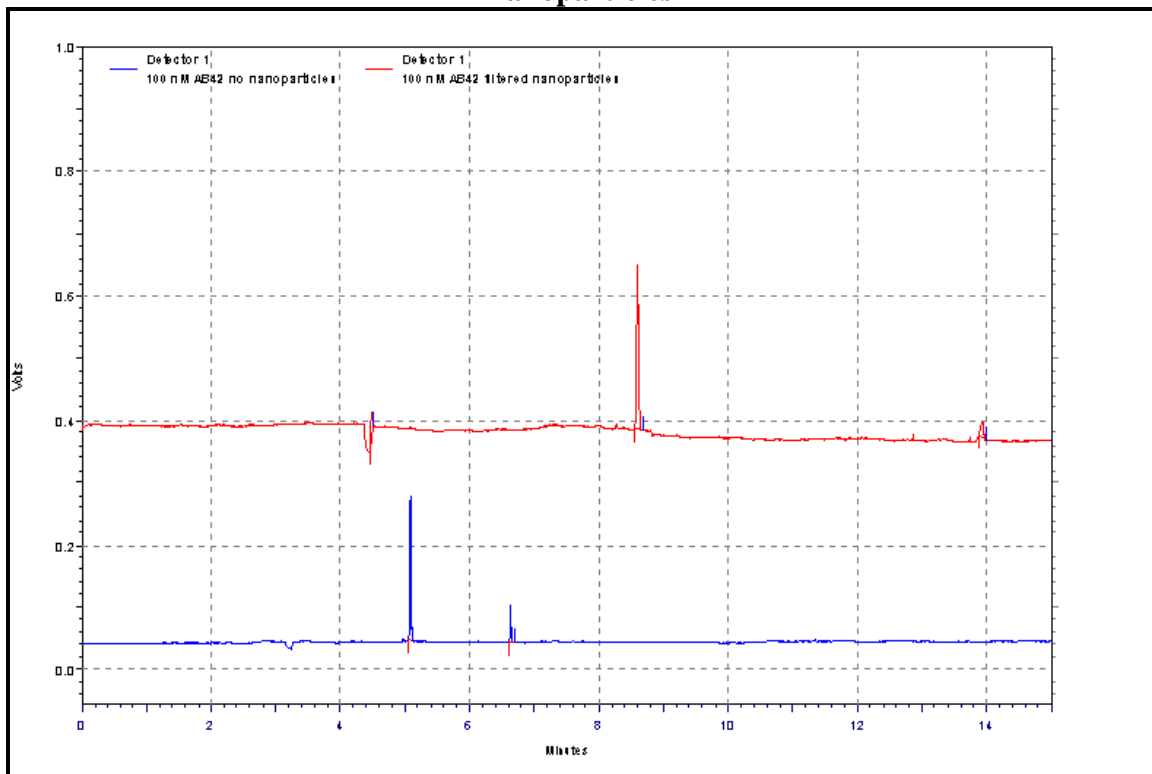**Figure 27. Electropherogram of AB42 (DyLight™) with/without functionalized nanoparticles**

Figure 28 shows the electropherograms for 10 nM tau both with and without nanoparticles. The bottom blue trace shows the analysis of tau that did not contain the nanoparticle pseudostationary phase. The protein is eluting after approximately 6 minutes. The top red trace shows the electropherogram of 10 nM tau protein in the CE analysis that did contain functionalized nanoparticles. The nanoparticles were shown to shift the elution time of the protein from 6 minutes to almost 11 minutes.

**Figure 28. Electropherogram of Tau (DyLight™) with/without functionalized nanoparticles**
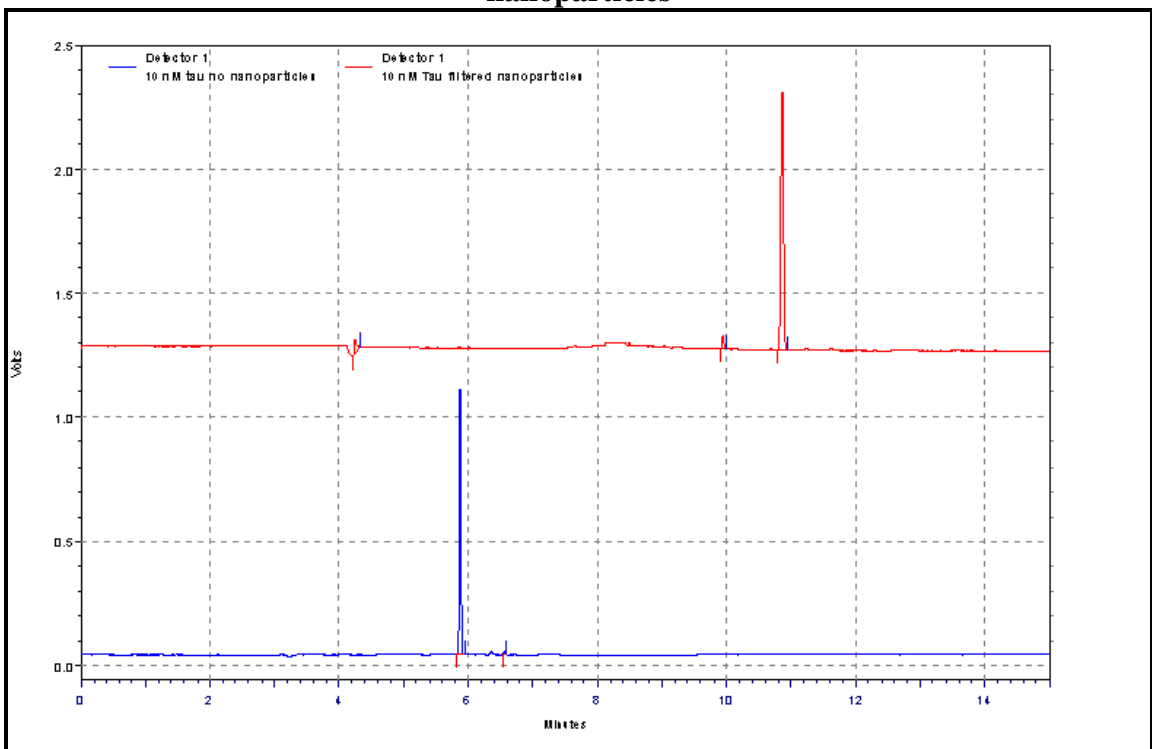
Despite displaying a delayed retention time in the presence of the functionalized gold nanoparticles, there was not enough interaction with the particles to separate the amyloid beta peptides. Because of this the pH and the applied voltage were both

decreased to increase the amount of time the analytes would spend in the capillary. At the lower pH there is a higher ratio of silanols that are protonated which decreases the bulk flow. The decrease in the voltage also decreases the electroosmotic flow because they are directly proportional. This decrease in the electroosmotic flow thereby increases the elution times of the analytes. In other words the analyte would have more time to interact with the nanoparticles. Even under these conditions, separation of the amyloid beta peptides was not achieved. It was believed that the size of the DyLight^{TM} dye was the main reason for this. The DyLight^{TM} dye adds approximately 1000 Da with each attachment. Since the peptides are only 4328 Da ($A\beta_{40}$) and 4514 Da ($A\beta_{42}$), the addition of such a large mass would decrease the difference in their charge to size ratios and decrease the differences in their polarity. The peptides were then derivatized with the smaller ATTO-TAG^{TM} FQ and run at the lower pH with lower applied voltage. The new buffer that was used was a 40 mM MES buffer at pH 5.00. This buffer was also used to suspend the nanoparticles to act as a pseudo stationary phase. The results of this analysis were somewhat surprising. Shown in Figure 29 is the electropherograms of 1 µM amyloid beta 40 (bottom blue trace), 1 µM amyloid beta 42 (second from bottom red trace), and 10 nM tau (top green trace), and a mixture of each of the biomarkers shown in the trace second from the top (pink trace). The analysis at lower pH appears to have allowed separation of the amyloid beta peptides without requiring the nanoparticle pseudostationary phase. Amyloid beta 40 is being shown to elute at around ten minutes. The slightly larger amyloid beta 42 eluted at 7.5 minutes. The tau protein is eluting at close to 16 minutes. While the separation under these conditions is surprising, the elution

order can be rationalized. At this pH the peptides are traveling as anions and are eluting after the electroosmotic flow. This fact was confirmed by determining the retention time of pure DMSO which acts as an electroosmotic flow marker. The peptides were shown to be eluting after this marker signifying that they are traveling as anions. Analytes with the same charge will then be separated by their mass. In this case since the amyloid beta 40 is smaller than amyloid beta 42 it has a greater electrophoretic mobility towards the inlet and therefore spends more time in the capillary. The tau protein is eluting last due to its greater mass.

Figure 29. Electropherogram of Alzheimer's Disease Biomarkers at pH 5
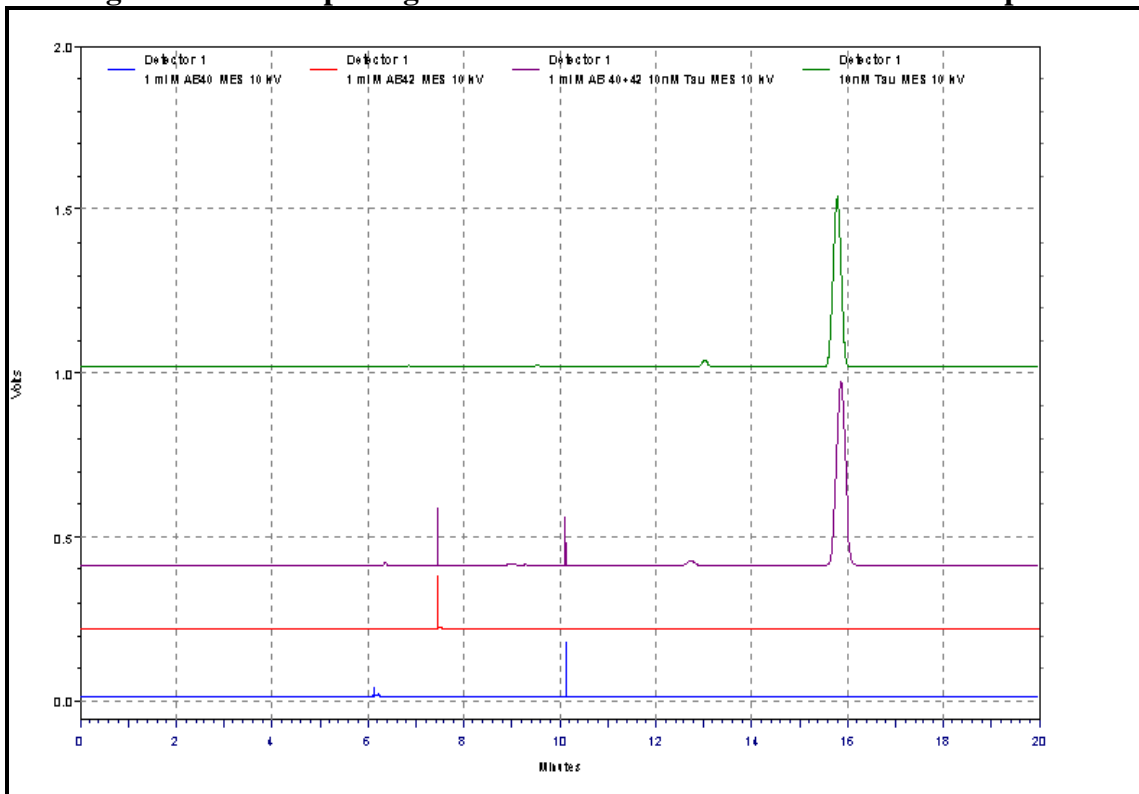
Despite being able to separate the biomakers in a buffer not containing nanoparticles, the analysis with nanoparticles was still performed. The conditions were identical to those of the previous analysis only the run buffer contained the functionalized gold nanoparticles. Figure 30 shows the results of this analysis. The blue trace on the bottom is 10 µM amyloid beta 40. It is being shown eluting at 16.8 minutes. The next trace up in red is 10 µM amyloid beta 42. This peptide elutes earlier at 11.3 minutes. Shown on top in green is the electropherogram of the 10 nM tau eluting after 24 minutes. The trace in purple shows the mixture of 10 µM amyloid beta 40, 10 µM amyloid beta 42 and 10 nM tau in a single analysis with each of the biomarkers' elution times corresponding to the individual analyses. It is important to note that there is an increase in the resolution of the biomarkers where the amyloid betas are separated by 5.25 minutes and the peptides are separated from the tau protein by approximately 7.25 minutes.

Figure 30. Electropherogram of Alzheimer's Disease Biomarkers at pH 5 with functionalized gold nanoparticles
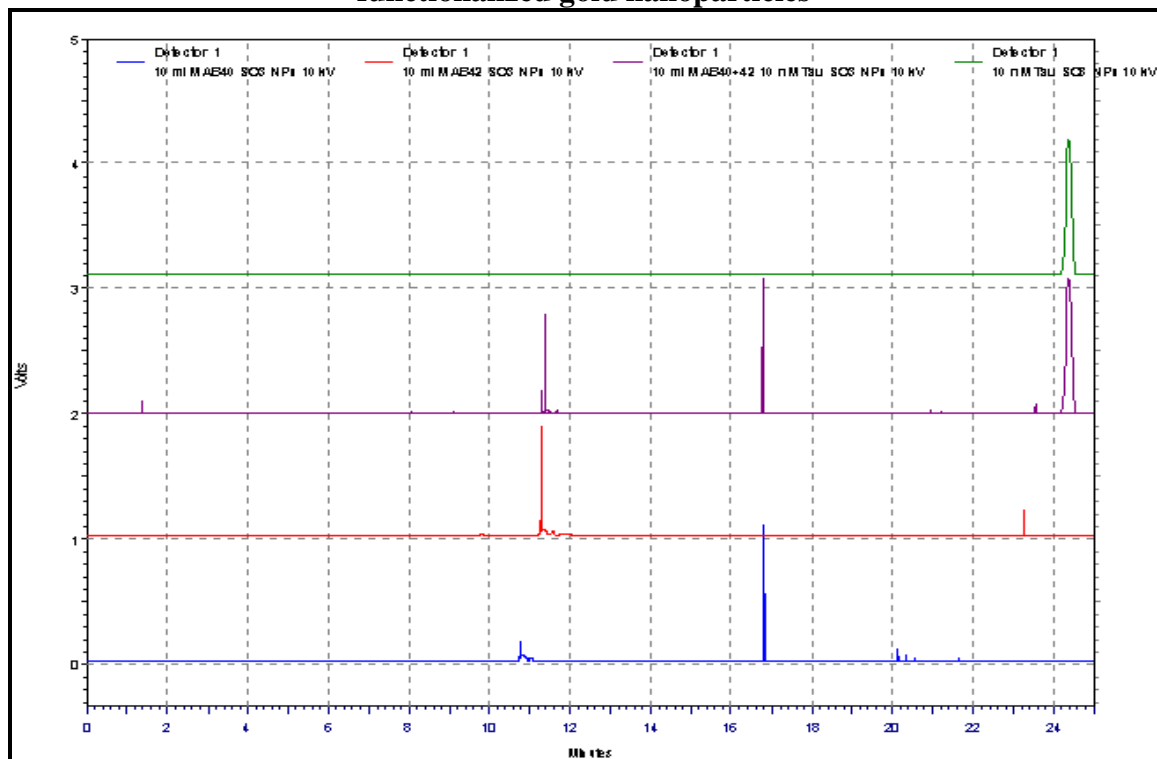
Conclusion

The use of the functionalized gold nanoparticle pseudostationary phase in a capillary electrophoretic analysis of Alzheimer's Disease biomarkers has enhanced the separation of the peptides allowing for quantitation. The initial dye that was used (DyLight[TM]) negated the slight difference in mass and polarity of the difficult to separate amyloid beta peptides. By using a smaller dye and slowing the electroosmotic flow by decreasing the pH of the run buffer and lowering the potential across the capillary, the separation of the amyloid beta peptides was achieved. The separation of the biomarkers allows for quantitation to be conducted. This implies that this type of analysis could be

conducted to determine the relative concentrations of the amyloid beta peptides and the

tau protein in a single analysis that would take approximately 2.5 hours including time

for the fluorescent derivatization of the biomarkers.

CHAPTER VII

CONCLUSION AND FUTURE WORK

Conclusion

This study achieved the synthesis and characterization of the asymmetric

disulfide, 10-(dodecyldisulfanyl) decane-1-sulfonic acid. The disulfide was characterized

through FTIR , ESI-MS, and NMR. This disulfide was then chemisorbed onto the

surface of 10 nm gold nanoparticles. The conditions for this derivatization were then

optimized for the concentration of the disulfide and reaction time of derivatization. Each

Alzheimer's Disease biomarker was then derivatized with a fluorescent dye so that they

could be detected in a capillary electrophoretic analysis using laser-induced fluorescence

detection. The pH of the fluorescent derivatization of the amyloid beta peptides was then

optimized to give the highest monodispersity in the molecular weights when analyzed by

MALDI-TOF MS. The fluorescently derivatized biomarkers were then analyzed by

capillary electrophoresis both with and without the functionalized gold nanoparticle

pseudostationary phase. The separation of the biomarkers was achieved at pH 5 at 10 kV

even without the presence of the nanoparticles. The analysis with the nanoparticles

exhibited increased separation between the amyloid beta peptides and the tau protein.

The resolution of Aβ40 and Aβ 42 was increased by 2.6 minutes, Aβ42 and tau was

increased by 4.6 minutes, and Aβ40 and tau was increased by 2.0 minutes. This

increased resolution would make future method development easier even in the presence

of interfering species. Both analyses with and without nanoparticles were completed

within 90 minutes including fluorescent derivatization of the biomarkers and the analysis

time. This technique provides a fast multianalyte analysis of the biomarkers in clean

media. What still remains is the analysis of these biomarkers in cerebrospinal fluid,

however, the high efficiency of capillary electrophoresis should be able to resolve these

biomarkers from interfering species present in the sample matrix.

Significance

Currently the only definitive diagnosis for Alzheimer's Disease is through an

autopsy to verify the presence of amyloid plaques and neurofibrillary tangles in the

patient's brain. Diagnosis of the disease involves ruling out the other forms of dementia

first then relying on tests of cognitive function and memory to determine if AD is the

cause. Also currently assisting in the diagnosis, is the use of Magnetic Resonance

Imaging (MRI) to provide evidence for brain atrophy due to neuronal loss.[53] It has been

shown that the relative concentrations of biomarkers such as $A\beta_{1-40}$, $A\beta_{1-42}$,

phosphorylated Tau (at threonine 181), and total Tau can be very useful in giving a more

accurate diagnosis. The only test that is utilized to determine the concentrations of these

biomarkers is ELISA. Analysis by ELISA is very time consuming and expensive

because each biomarker would require a separate analysis. The results of ELISA tests

have been shown to be widely variable.[54] Probably one of the biggest drawbacks to an

ELISA analysis is the problem of accuracy. These are known to be inaccurate at

correctly determining analyte concentrations. A CE analysis could invoke the use of an

internal standard to help verify the relative concentrations. This study proposed the use

of capillary electrophoresis for the separation of these biomarkers. CE experiments are

often very fast (around 10 minutes) and consume very little sample (~3-5 nL). The

knowledge of the relative concentrations of the biomarkers could lead to a faster and

more accurate diagnosis of the disease. It would also provide a means of tracking

progression of the disease to determine the efficacy of various treatments.

Future Work

From here this analysis can provide information that is imperative to diagnosing

Alzheimer's disease. Work should be done to decrease the detection limits of the

biomarkers so that biologically relevant concentrations of the biomarkers can be detected.

Future studies should also include the quantitation of the phosphorylated form of the tau

protein to provide a complete description of the disease progression.

REFERENCES

[1] Wang, D. S.; Dickson, D. W.; Malter, J. S. *J Biomed Biotechnol* **2006,** *2006* (3), 58406.

[2] Mattsson, N.; Zetterberg, H.; Hansson, O.; Andreasen, N.; Parnetti, L.; Jonsson, M.; Herukka, S.; van der Flier, W.; Blankenstein, M.; Ewers, M.; Rich, K.; Kaiser, E.; Verbeek, M.; Tsolaki, M.; Mulugeta, E.; Rosén, E.; Aarsland, D.; Visser, P.; Schröder, J.; Marcusson, J.; de Leon, M.; Hampel, H.; Scheltens, P.; Pirttilä, T.; Wallin, A.; Jönhagen, M.; Minthon, L.; Winblad, B.; Blennow, K. *JAMA* **2009,** *302* (4), 385-93.

[3] U.S. Department of Health and Human Services, AD research advances: Many paths to the goal, **2005-2006** progress report on Alzheimer's disease.

[4] Ferri, C. P.; Prince, M.; Brayne, C.; Brodaty, H.; Fratiglioni, L.; Ganguli, M.; Hall, K.; Hasegawa, K.; Hendrie, H.; Huang, Y.; Jorm, A.; Mathers, C.; Menezes, P. R.; Rimmer, E.; Scazufca, M. *Lancet* **2005,** *366* (9503), 2112-7.

[5] Harris, D. C., *Quantitative chemical analysis*. 7th ed.; W.H. Freeman and Co.: New York, NY, 2007; p 1 v. (various pagings).

[6] Guo, Y.; Imahori, G. A.; Colon, L. A. *J Chromatogr A* **1996,** *744* (1-2), 17-29.

[7] Landers, J. P., *Handbook of capillary electrophoresis*. 2nd ed.; CRC Press: Boca Raton, **1997**; p 894.

[8] Wang, T.; Aiken, J. H.; Huie, C. W.; Hartwick, R. A. *Anal Chem* **1991,** *63*, 1372-6.

[9] Timperman, A. T.; Khatib, K.; Sweedler, J. V. *Anal Chem* **1995,** *67* (1), 139-44.

[10] Hernandez, L.; Joshi, N.; Escalona, J.; Guzman, N. *J Chromatogr A* **1991,** *559*, 183-196.

[11] MacTaylor, C. E.; Ewing, A. G. *Electrophoresis* **1997,** *18* (12-13), 2279-90.

[12] Pinto, D. M. *Anal Chem* **1997,** *69*, 3015-21.

[13] Zhao, J.; Chen, D. Y.; Dovichi, N. J. *J Chromatogr A* **1992,** *608*, 117-20.

[14] Zhang, L.; Yeung, E. S. *J Chromatogr A* **1996,** *734*, 331-7.

[15] Kuhr, W. G.; Yeung, E. S. *Anal Chem* **1988,** *60* (17), 1832-4.

[16] Mazereeuw, M.; Hofte, A. J.; Tjaden, U. R.; Van der Greef, J. *Rapid Communications in Mass Spectrometry* **1997,** *11*, 561-4.

[17] Zhang, H.; Caprioli, R. M. *J Mass Spectrom* **1996,** *31* (9), 1039-46.

[18] Terabe, S.; Otsuka, K. *Anal Chem* **1985,** *57*, 834-41.

[19] Koezuka, K.; Ozaki, H.; Matsubara, N.; Terabe, S. *J Chromatogr B Biomed Sci Appl* **1997,** *689* (1), 3-11.

[20] Jorgenson, J. W.; Lukacs, K. D. *J Chromatogr A* **1981,** *218*, 209-16.

[21] Knox, J. *Chromatographia* **1988,** *26*, 329-37.

[22] Lin, S.; Tsai, Y.; Chen, C.; Lin, C.; Chen, C. *J Phys Chem B* **2004,** *108*, 2134-9.

[23] Nuzzo, R. G.; Allara, D. L. *J Am Chem Soc* **1983,** *105*, 4481-3.

[24] Ulman, A. *Chem Rev* **1996,** *96* (4), 1533-1554.

[25] Bain, C. D.; Troughton, E. B.; Tao, Y.; Evall, J.; Whitesides, G. M. *J Am Chem Soc* **1989,** *111*, 321-35.

[26] Biebuyck, H. A.; Whitesides, G. M. *Langmuir* **1993,** *9*, 1766-70.

[27] Bain, C. D.; Biebuyck, H. A.; Whitesides, G. M. *Langmuir* **1989,** *5*, 723-7.

[28] Shon, Y. S.; Mazzitelli, C.; Murray, R. W. *Langmuir* **2001,** *17*, 7735-41.

[29] Kelly, K. L.; Coronado, E.; Zhao, L.; Schatz, G. *J. Phys. Chem. B* **2003,** *107*, 668-677.

[30] Jain, P. K.; Huang, X.; El-Sayed, I. H.; El-Sayed, M. A. *Acc Chem Res* **2008,** *41* (12), 1578-86.

[31] Jain, P. K.; Huang, X.; El-Sayed, I. H.; El-Sayed, M. A. *Plasmonics* **2007,** *2*, 107-118.

[32] Jain, P. K.; Lee, K. S.; El-Sayed, I. H.; El-Sayed, M. A. *J Phys Chem B* **2006,** *110* (14), 7238-48.

[33] Hostetler, M. J.; wingate, J. E.; Zhong, C. J.; Harris, J. E.; Vachet, R. W.; Clark, M. R.; Londono, J. D.; Green, S. J.; Stokes, J. J.; Wignal, G. D.; Glish, G. L.; Porter, M. D.; Evans, N. D.; Murray, R. W. *Langmuir* **1998,** *14*, 17-30.

[34] Badia, A.; Demers, L.; Morin, F. G.; Lennox, R. B.; Reven, L. *J Am Chem Soc* **1997,** *119*, 11104-5.

[35] Hostetler, M. J.; Stokes, J. J.; Murray, R. W. *Langmuir* **1996,** *12*, 3604-12.

[36] Ferri, C. P.; Prince, M.; Brayne, C.; Brodaty, H.; Fratiglioni, L.; Ganguli, M.; Hall, K.; Hasegawa, K.; Hendrie, H.; Huang, Y.; Jorm, A.; Mathers, C.; Menezes, P. R.; Rimmer, E.; Scazufca, M. *Lancet* **2005,** *366* (9503), 2112-7.

[37] Walsh, D. M.; Klyubin, I.; Fadeeva, J. V.; Cullen, W. K.; Anwyl, R.; Wolfe, M. S.; Rowan, M. J.; Selkoe, D. J. *Nature* **2002,** *416* (6880), 535-9.

[38] Hoshi, M.; Sato, M.; Matsumoto, S.; Noguchi, A.; Yasutake, K.; Yoshida, N.; Sato, K. *Proc Natl Acad Sci U S A* **2003,** *100* (11), 6370-5.

[39] Guo, J. P.; Arai, T.; Miklossy, J.; McGeer, P. L. *Proc Natl Acad Sci U S A* **2006,** *103* (6), 1953-8.

[40] Johnson, G. *Alzheimer's Disease* **2006,** *9*, 243-50.

[41] Kopke, E.; Tung, Y. C.; Shaikh, S.; Alonso, A. C.; Iqbal, K.; Grundke-Iqbal, I., *J Biol Chem* **1993,** *268* (32), 24374-84.

[42] Avila, J., *FEBS Lett* **2006,** *580* (12), 2922-7.

[43] Blennow, K.; de Leon, M. J.; Zetterberg, H. *Lancet* **2006,** *368* (9533), 387-403.

[44] Wiltfang, J.; Esselmann, H.; Bibl, M.; Hull, M.; Hampel, H.; Kessler, H.; Frolich, L.; Schroder, J.; Peters, O.; Jessen, F.; Luckhaus, C.; Perneczky, R.; Jahn, H.; Fiszer, M.; Maler, J. M.; Zimmermann, R.; Bruckmoser, R.; Kornhuber, J.; Lewczuk, P. *J Neurochem* **2007,** *101* (4), 1053-9.

[45] 1. Sunderland, T.; Linker, G.; Mirza, N.; Putnam, K. T.; Friedman, D. L.; Kimmel, L. H.; Bergeson, J.; Manetti, G. J.; Zimmermann, M.; Tang, B.; Bartko, J. J.; Cohen, R. M. *JAMA* **2003,** *289* (16), 2094-103.

[46] Ulman, A. *Chem Rev* **1996,** *96* (4), 1533-1554.

[47] Fiurasek, P.; Reven, L. *Langmuir* **2007,** *23* (5), 2857-66.

[48] Brocklehurst, K.; Carlsson, J.; Kierstan, M. P.; Crook, E. M. *Methods Enzymol* **1974,** *34*, 531-44.

[49] Margelefsky, E. L.; Bendjeriou, A.; Zeidan, R. K.; Dufaud, V.; Davis, M. E. *J Am Chem Soc* **2008,** *130* (40), 13442-9.

[50] Nuzzo, R. G.; Allara, D. L. *J Am Chem Soc* **1983,** *105*, 4481-3.

[51] Grasso, G.; Mineo, P.; Rizzarelli, E.; Spoto, G. *Int J Mass Spectrom* **2009,** *282*, 50-55.

[52] Reijenga, J. C. *Encyclopedia of Chromatography* 3rd ed.; CRC Press: Boca Raton, **2010**; (1) 124.

[53] Schott, J. M.; Kennedy, J.; Fox, N. C. *Curr Opin Neurol* **2006,** *19* (6), 552-8.

[54] Fukuyama, R.; Mizuno, T.; Mori, S.; Nakajima, K.; Fushiki, S.; Yanagisawa, K., *Eur Neurol* **2000,** *43* (3), 155-60.